Karlsruhe Institute of Technology

A Comparative Analysis of Switchings in Static and Dynamic Power Grids

Master Thesis of

Adrian Grupp

At the Department of Informatics
Institute of Theoretical Informatics

Reviewers:	Dr. Torsten Ueckerdt, Prof. Dr. Dorothea Wagner
	Prof. Dr. Peter Sanders
Advisors:	Franziska Wegner
	Matthias Wolf

Time Period: 1st July 2019 – 4th April 2020

Acknowledgments

I wish to thank Prof. Dr. Veit Hagenmeier at IAI KIT for providing valuable knowledge and material on the modeling and analysis of power grids and dynamical systems.

Statement of Authorship

I hereby declare that this document has been composed by myself and describes my own work, unless otherwise acknowledged in the text.

Karlsruhe, October 3, 2020

Abstract

The power grid is the largest machine humankind has ever built. However, this machine is facing wide-ranging structural change. The transition towards intensive usage of renewable energy sources introduces new challenges: How do we cope with their volatility and how can we use them as efficiently as possible? Exploiting structural properties may be one answer to this.
On one hand it is known that purposefully removing transmission lines from a power grid, so called *switching*, can in fact resolve congestions and overloads, which can eventually lead to a higher power throughput. In the language of graph theory this can be formalized as an optimization problem on flow networks, the Maximum Transmission Switching Flow Problem.
On the other hand the concern is that the power grid can be compromised by such big topological interventions as the removal of a whole transmission line. Stable operation has to be guaranteed at all times which means adhering to the network's utility frequency. The *oscillator model*, used in statistical physics, can be utilized to study the transient behavior of the power grid. With it we can investigate whether switchings still allow network *synchronization*. Additionally, small signal analysis can be used to analyze the stability of the system after the switching took place.

In this work we give a comparative analysis of the two mentioned approaches. We study how optimization results from the static world of graph theory behave in the dynamic setting of real world power grids and assess if they are reasonable with regards to the stability of the network frequency. We want to shed light on the derivation of the models and give a first answer to the question whether we can safely use switching in order to improve our power grids.

Deutsche Zusammenfassung

Das Stromnetz ist die größte Maschine, die die Menschheit jemals gebaut hat. Allerdings steht diese Maschine vor weitreichenden Veränderungen. Mit dem Übergang zu einer intensiveren Nutzung erneuerbarer Energien kommen einige Herausforderungen: Wie können wir mit deren Unbeständigkeit umgehen und wie können wir sie so effizient wie möglich nutzen? Das ausnutzen struktureller Eigenschaften könnte eine Antwort darauf liefern.
Auf der einen Seite ist bekannt, dass man mit dem gezielten Entfernen von Übertragungsleitungen, sogenanntem *Switching*, tatsächlich Verstopfungen und Überlasten verhindern kann, was wiederum zu einem größeren Leistungsdurchsatz führt. Graphentheoretisch ausgedrückt kann dies als ein Optimierungsproblem auf Flussnetzwerken formuliert werden, dem Maximum Transmission Switching Flow Problem.
Andererseits existiert die Sorge, dass das Stromnetz durch so umfangreichen Einwirkungen, wie das zeitweise entfernen ganzer Übertragungsleitungen, Schaden davon tragen kann. Ein sicherer Netzbetrieb, um genau zu sein das Halten der Netzfrequenz, muss zu jedem Zeitpunkt garantiert werden. Physikalisch ausgedrückt: Ist die *Synchronisation* im Netzwerk immer gewährleistet? Das *Oszillator Modell* aus der statistischen Physik ist ein Werkzeug um eben dieses Verhalten zu untersuchen. Zusätzlich können wir Kleinsignalanalyse verwenden, um kritische Zeitpunkte während des Switching-Vorgangs zu untersuchen.

In dieser Arbeit stellen wir eine vergleichende Analyse der zwei erwähnten Ansätze an. Wir untersuchen, inwiefern Optimierungen aus der statischen Betrachtungsweise der

Graphentheorie in der dynamischen Welt echter Stromnetze genutzt werden können und bewerten, ob diese im Bezug auf die Stabilität der Netzfrequenz sinnvoll sind. Wir wollen Licht die auf Herleitung der Modelle werfen und eine erste Antwort darauf geben, ob Switchings eingesetzt werden können, um unser Stromnetz zu verbessern, ohne es dabei zu beschädigen.

Contents

1. Introduction

Robustness and efficient operation of critical infrastructures, such as telecommunication, transportation and water or electricity supply are the key prerequisites for the functioning of our modern society. Satisfying them is becoming a more and more challenging task. This is especially true for power distribution and transmission. With society's growing hunger for power on the one side and the aim to get rid of the enormous carbon footprint of conventional energy production on the other, a shift towards renewable energy sources is inevitable.
However, their increasing share on the energy market leads to new challenges and an operational paradigm shift. Renewables are harvested in a more decentralized manor and in different geographical locations. Offshore wind farms are located in remote areas, while photovoltaics allow each individual person to produce power and inject it to the power grid wherever they live. So instead of a few power stations with central positions in the grid there are now many power producers spread across it, providing a wide range of energy input. One arising problem here is that there is no active control concerning all the smaller power sources to regulate them according to the currently present energy consumption. This trend is only going to advance in the future with efforts aiming at carbon neutral power production such as the 'Energiewende' in Germany [PAH14].
Furthermore, power from renewable sources does not come in consistent rates, but can heavily fluctuate due to factors such as weather changes. Peaks of heavy production as well as periods of low winds or no sun light make the task of providing a stable operation of the power grid more problematic [HvBG+10]. Transmission lines may be congested and even get damaged due to transgression of their thermal limits. It is therefore mandatory to explore and refine possible solutions for these emerging challenges in order to guarantee the reliable operation of this key infrastructure of our modern world.

As a power grid plays such a critical role for our society and is operating around the clock, simply trying out solutions and modifications is not a viable option, as interventions can have wide-ranging consequences. In order to tackle the described problems we therefore need a proper way to model it. There are several layers of abstraction and coarseness we can look at. In this work we study high-level approaches that aim at the topology and stability properties of the transmission grid. The choice of *how* implies *what* can actually be modeled. Static models for optimization algorithms for example are not capable to capture the transient behavior. When looking at the grid from a high-level perspective there are several criteria one may be interested in: making the grid more stable or redundant,

increase its throughput or identify critical parts that may be prone to attacks or overload in the future.

The obvious way to add redundancy is by installing additional network infrastructure. This however is a costly endeavor and construction projects often face opposition [mdr19]. Another way to account for congested transmission lines therefore is to temporarily remove transmission lines purposefully from the grid in order to actually increase throughput. This method is called *switching*. A graph-theoretic representation of the power grid using flow networks turns out to be a useful way to analyze topological properties of it and find optimal switching positions. In this work we take a look at the results of Grastien et al. [GRW+18]. The authors use a flow network extended with physical properties for finding optimal *power flows* with switching and give complexity bounds for certain scenarios.

However, the graph-theoretic model has a drawback. It is just a static representation of the transmission network. This means we only observe one 'snap shot' in time and cannot express more complex behavior such as the transience after a transmission line got switched out. This can lead to unforeseen consequences and threaten network operation [faz06]. Hence, it is not enough to solely optimize the power throughput. We want to analyze how power grids behave over a certain time and what effect interventions such as switching may have. The mathematical property to describe a stable operation of a network is the *synchronization* between the involved units. The framework of *coupled oscillators* [FNP08] has proven to be a valuable tool for modeling the dynamic behavior of power grids. The representation via ordinary differential equation allows us to see how switching and other network perturbations (e.g. change in network load) affect the network stability over time.

1.1. Related Work

The analysis of power grids and ways to model it has always been of great importance for smooth and efficient operation. In recent years research in this field advanced a lot as it has to tackle a lot of new issues caused by the drastic changes happening due to the shift to renewable energy and growing power demand. The aspects to analyze and the properties to model in a power grid are numerous. Rhoden et al. [RSTW12] pin down two types of approaches when studying them. On the one hand there is the detailed component based approach of electrical and power engineering, giving very precise simulations. It allows for close investigation of the nonlinear dynamic behavior present in AC power grids. Although more realistic, this approach comes at the cost of a lot of parameters to take into account. The other approach is more abstract and coarse grained, looking at the power grid as a network with buses and branches as smallest components. It allows for a large-scale analysis, however only allowing a static topological view with no dynamics involved. Additionally, the authors also discuss a third method that tries to combine nonlinear dynamics with the large-scale approach. In this work we look at the latter two.

Some of the most essential equations that capture the operation of power grids are the *load-flow* equations [Sto74]. Calculating their numerical solutions is a key task for dispatching power properly to the transmission network. The model based on these equations is called the *AC model*, as it describes the nonlinear behavior of alternating current (AC). A simplified version of the AC model is retrieved by linearizing the power flow equations. The resulting, so-called *linear DC model* [SR70] behaves much like direct current (DC), hence the name. In his work Schweppe presents the main underlying assumptions of small line resistance, flat voltage profiles and small voltage angle differences which allows for significant simplifications of the power flow formulation.

Purchala et al. [PMVB05] later showed that certain problems can arise when applying these simplifying assumptions and that reliability can only be expected when modeling the high voltage layer of the grid. However, in this case they prove to be a good approximation that allow for more feasible computations.

For load flow studies the MATPOWER [ZMsT+11] platform provides tools and datasets of power grids as well as a comprehensive derivation of the underlying algorithms. The NICTA Energy System Test Case Archive (NESTA) [CGS14] provides a collection of refined case files e.g. from the MATPOWER or IEEE platform [UoW14].

Network Optimizations

Augmenting the power grid for the future challenges provided by renewable energies can be approached from several directions. One is transmission network expansion planning [GMM92, BPG01]. Adding more transmission lines and circuits may provide redundancy in case of overload scenarios by increasing transmission capacities. Yet, this approach requires heavy construction effort and is rather expensive.
Placing Flexible AC Transmission Systems (FACTS) [LMM+15, LGHV15] in the existing grid can be used to alter the line susceptance and also potentially resolves overload scenarios. This does not require new transmission lines, but still is a costly investment and hence finding optimal and as few as possible placements is crucial.

Another approach is based on an observation originally made in traffic networks. Already in 1968 Dietrich Braess discovered that adding additional roads can actually lead to worse over-all commute times [Bra68]. Having new connections may cause congestions in parts of the network that are not capable of handling an increase in traffic. This phenomenon is nowadays coined *Braess's Paradox*. It can also be connected to power grids [Blu06] and gives the prime motivation to apply *switching*. Switching is the temporary removal of transmission lines using switches such as circuit breakers in order to increase the power flow. Fisher et al. [FOF08] found, using a mixed-integer linear program that switchings can in fact improve prower grid operation and saw a reduction of up to 25% in generator dispatch cost. Finding optimal operational costs via switchings is known as the OPTIMAL TRANSMISSION SWITCHING PROBLEM. This means minimizing the generation cost while satisfying a given power demand.

Graph-Theoretic View

It is obviously convenient to represent a power grid's buses and transmission lines with a graph. Especially when it comes to structural considerations as mentioned above. Graph-theoretical results on the complexity of power engineering problems help to classify them. A common way is to consider flow networks in which we can embed the load flow.
Prominent problems are the feasibility problem (FEAS) which requires to find a power flow serving all loads while satisfying the capacity constraints on the transmission lines. The MAXIMUM POWER FLOW PROBLEM (MPF) asks for the highest power flow possible. Moreover, the MAXIMUM TRANSMISSION SWITCHING FLOW (MTSF) asks for the maximum value when we allow for switchings.

Finding optimal solutions to these problems is difficult. Lehman et al. [LGV16] for example show that the feasibility problem for AC networks is NP-hard already on star networks. Using the DC approximation they also show that finding optimal power flows and maximum transmission switching flows are NP-hard problems on limited graph classes [LGV14]. For general graphs they cannot even be approximated within any constant factor. The authors furthermore extend their findings in [LGHV15] to show that MPF is not only NP-complete under switchings but also when placing FACTS.

Grastien et al. [GRW+18] provide more insight into the structural properties of the MTSF problem. Their formulation of *dominating theta paths* allows for MTSFs on penrose-minor free graphs with one generator and one load and is suggested as a heuristic for general graphs representing power grids. They furthermore provide a 2-approximation for cactus graphs.

Finding the maximal power flow with switchings is actually a subproblem of the *power system restoration* problem [Adi00]. It asks for the choice of transmission lines to be repaired first after a disaster in order to restore as much power transmission as quickly as possible.

Transient Analysis

While graph-theoretic approaches and linearization assumptions may give good insights into the mentioned problems and how to solve them, a power grid remains a dynamical system with nonlinear interactions happening and evolving over time. Applying changes to its topology may destroy the stability of its operation. Kundur et al. [KPA+04] give a classification of different kinds of network stability - rotor angle, voltage and frequency stability. *Transient analysis* looks at the system in order to determine whether perturbing or altering the network may destroy that stability.

Dynamical systems however cover an even wider range of real world processes from pendulums, to predator-prey-behavior up systems as complex as climate models. The aim is to harness findings and theories from this interdisciplinary field.
One very important property emerging in dynamical networks is synchronization. The interaction between network components is described by coupled oscillators that synchronize their oscillations when in a stable state. One of the most versatile models to study how, when and why this happens is the *Kuramoto model* [Kur75]. Over the years it has seen applications in biology [MV06], chemistry [Kur03], seismology, neuronal Networks and many more fields [RPJK16].

In 2008 Filatrella [FNP08] was the first to connect power grids with the Kuramoto model. By representing power generators and loads with the oscillator equations he was able to study the system behavior after perturbations such as load spikes took place. The system however becomes more complex as damping and inertia also play a role in a generator's behavior.

There have been several successful applications ever since. Witthaut et al. [WT12] demonstrate that Braess' Paradox is present in oscillator networks as well and link it to geometric frustration. Rhoden et al. [RSTW12] study how self organized synchronization happens in decentralized power grids. Their findings are that decentralization, e.g., due to renewable energy production increases sensitivity to perturbations but also increases robustness regarding topological changes.

The *criticality* of a transmission line means how sensitive the network synchronization reacts to the removal of this link [Win19]. Lozano et al. found in [LBDG12] that the loss of transmission lines connecting national power grids is often more prone to desynchronizing. They link transient behavior to network topology, as transboundary power grids tend to be clustered per nation. Criticality and flow redistribution is also studied in [WRZ+16a].

Motter & Lai [ML02] show how redistribution after a line outage can lead to a cascade of failures as the overload propagates through the network. This is what happens during major blackouts. Works such as [RJTK16] and [SWTL18] further investigate this phenomenon using the oscillator model.

Cascading failures have also been studied using an other approach stemming from statistical physics. Simonsen et al. [SAMS04, Sim05] establish a connection between diffusion

processes on networks and random walks. Flow can be understood as many random walkers moving randomly along a network's edges. This induces a current by the probabilities of taking a certain direction. Later the model was used for transient analysis [SBP+08] on power grids. The findings suggested a connection between cascading failures and line capacities.

Direct methods allow for an immediate assessment of the system stability after a fault or switching took place. They do not require numerical integration but make use of Lyapunov's first and second method [APV79]. Another method, the equal area criterion and Lyapunov's method are discussed in [WJSO12] for real time applicability to transient stability analysis. Finally, Kyesswa et al. present a hybrid method [KCG+19], combining the efficiency of direct methods with the power to derive the system trajectory of numerical integration.

1.2. Contribution

In this work we give first answers to the questions whether we we can use the switching heuristics based on dominating theta paths proposed in [GRW+18] and if a stable operation of the power grid is possible afterwards. We present the linear DC model with its underlying assumptions and how it is put to use on graph-theoretic flow networks to find MTSFs. We show limitations of such a static representation and give a detailed derivation of the oscillator model as a dynamic counterpart. Based on it we use small-signal analysis in order to get insights into the networks' stability and numerical integration for the synchronization behavior after switching out an edge. We carry out our analysis on the NESTA case files. The static heuristic from Grastien et al. gives a new notion of centrality based on dominating theta path betweenness, denoted by c_{DTPB} and gives an ordering on the edges suggesting which one to switch for an MTSF. We connect this to dynamical properties such as the change of a network's frequency amplitudes and load redistribution. We can show proportional behavior in a lot of cases and point out reasons for the scenarios in which such a correspondence could not be found. Applying small-signal analysis our findings are that edge switchings with smaller c_{DTPB}-values are more likely to leave the system in an unstable state. The highest c_{DTPB}-value on the other hand almost always leaves the network in an operable state. We conclude that that edges with a higher centrality in many cases lead to less severe system disruption. We also identify a special case where the network behaves highly instable and the heuristic seems not to work as well. We can link this behavior to its topological properties, namely many tree-like subgraphs that disconnect the network for a lot of switchings. This eventually leads to more load redistribution and worse synchronization behavior.
Finally, we also look at the mean-field values [Str00] of the power grids as another measure for the transient behavior after switching. Again, we observe that in most cases a lower c_{DTPB}-value can be linked to a reduced coherence between the network's oscillations.

1.3. Outline

The rest of this work is structured as follows. Chapter 2 Gives an overview of the mathematical and technical background of this work. It provides the a brief introduction to concepts from graph theory, electrical and power engineering and ordinary differential equations. In Chapter 3 we present the derivation of the linear DC model. We then give the graph-theoretic representation of the power flow using flow networks. A definition of the Maximum Transmission Switching Flow Problem and a power flow specific centrality measure are given. The second approach to model a power network is provided in Chapter 4 where we introduce the oscillator model. We look at its derivation, and

properties such as synchronization and steady states. Chapter 5 describes the procedures we used to analyze a power grid under switching. Small-signal analysis, according to Lyapunov's first method is explained as well as numeric integration that is used for the calculation of solutions to the oscillator equations. We present our evaluation results in Chapter 6. Here we build the connection between the derived heuristics from the graph model and the stability results of the transient analysis. We show how switchings could affect the network and discuss correlations in the observed behavior. Finally, a conclusion of the work and a prospect on further steps is given in Chapter 7.

2. Preliminaries

2.1. Graph Theory

In this section we introduce some basic graph-theoretic notation and define flow networks.

Definition 2.1 (Undirected Graph [Die05])**.** *An* undirected graph *is a pair* $G = (V, E)$ *of sets, where* $V = \{v_1, v_2, ...v_n\}$ *is the set of* nodes *with* $n \in \mathbb{N}$ *and* $E \subseteq \{\{u, v\} \mid u, v \in V\}$ *the set of* undirected edges*.*

Definition 2.2 (Directed Graph [Die05])**.** *A* Directed graph *is a pair* $\vec{G} = (V, \vec{E})$ *of sets with* $V = \{v_1, v_2, ...v_n\}, n \in \mathbb{N}$ *and the elements of* $\vec{E} \subseteq \{(u, v) \mid u, v \in V\} = V \times V$ *are called* directed edges*. For an edge* $e = (u, v) \in \vec{E}$ *we call* u from-node *and* v to-node*.*

In the case of a directed graph $\vec{G} = (V, \vec{E})$, the set of *incoming* edges at a node v is defined by $\delta^+(v) \coloneqq \{e = (u, v) \in \vec{E} \mid u \in V\}$ and the set of *outgoing* edges is $\delta^-(v) \coloneqq \{e = (v, u) \in \vec{E} \mid u \in V\}$.

In this work we are often interested in graphs whose edges have a direction. However, the original graph we are provided with may be undirected, as it is the case with power grid datasets. The following definition gives an equivalent representation of an undirected graph as one with directed edges. The idea is to replace every undirected edge $e = \{u, v\} \in E$ in the graph with two directed edges $(u, v), (v, u) \in \vec{E}$, pointing towards opposite nodes.

Definition 2.3. *Let* $G = (V, E)$ *be an undirected graph. Define* $\vec{E} \coloneqq \{(u, v), (v, u) \mid \{u, v\} \in E\}$ *and* $\vec{G} = (V, \vec{E})$*. Such a graph* $\vec{G}$ *is called* bi-directed*.*

This construction can be applied in the opposite direction analogously.

Definition 2.4 (Subgraph [Die05])**.** *Let* $G = (V, E)$ *be an undirected graph. If* $V' \subseteq V$ *and* $E' \subseteq E$ *then we call* $G' = (V', E')$ *a* subgraph *of* G *and write* $G' \subseteq G$*.*

The definition for subgraphs of directed graphs is analogous.

As we want to study how power in a power grid is transmitted from A to B we need to add some properties to the graph in order to express this. *Networks* are used to model how units of some good are passing from some source node of the graph to a destination via the edges, while constraining their capacity.

Definition 2.5 (Network)**.** *Let $G = (V, E)$ be a graph and $\vec{G} = (V, \vec{E})$ its bi-directed corespondent, $s, t \in V, s \neq t$ two unique nodes and $cap : \vec{E} \to \mathbb{R}_{\geq 0}$ a map. The tuple $\mathcal{N} = (\vec{G}, s, t, cap)$ is then called* network*. We refer to s as* source *and t as* sink *of the network and call cap the* capacity function*.*

This definition can be generalized by replacing s and t with (disjoint) sets of sources $S \subseteq V$ and sinks $T \subseteq V$ respectively and requiring $S \cap T = \emptyset$.

Next, we define a function on the edges of the network's graph that expresses how many units move along them. It has to satisfy three properties:

1. *Skew symmetry*: What is send into one direction has to be equated by the corresponding negative value on the edge going towards the other directions (Equation (2.1)).
2. *Flow conservation*: Nodes that are not sources or sinks have to send out as much as they receive (Equation (2.2)).
3. *Capacity constraint*: It is illegal to send more units over an edge than its capacity allows for (Equation (2.3)).

A function satisfying these constraints is called a *feasible flow* or just *flow* and is formally defined as follows:

Definition 2.6 (Flow[Die05])**.** *Let $\mathcal{N} = (\vec{G}, S, T, cap)$ be a network. The function $f : \vec{E} \to \mathbb{R}$ on the directed edges of G is called a* feasible flow *or just* flow *if it satisfies the following three conditions:*

$$f(u, v) = -f(v, u) \qquad , \forall (u, v) \in \vec{E} \tag{2.1}$$

$$\sum_{e \in \delta^+(v)} f(e) = \sum_{e \in \delta^-(v)} f(e) \qquad , \forall v \in V \setminus S \cup T \tag{2.2}$$

$$|f(e)| \leq cap(e) \qquad , \forall e \in \vec{E} \tag{2.3}$$

An important subclass of graphs are *paths*, going from one vertex to another. We provide the definition based on undirected graphs but the one for directed graphs again is analogous with respect to the edge directions.

Definition 2.7 (Path [Die05])**.** *A* path *is a graph $P = (V, E)$ of the form $V = \{v_0, v_1, \ldots, v_k\}$, $E = \{\{v_0, v_1\}, \{v_1, v_2\} \ldots \{v_{k-1}, v_k\}\}$ s.t. all v_i are distinct. We denote it by $\pi(v_0, v_k)$ and call it a path from v_0 to v_k.*

In this work we look at paths as subgraphs of networks and hence are interested in the set of all paths that lead from one node to another.

Definition 2.8. *Let $G = (V, E)$ be an undirected graph. We denote the set of all paths from v_0 to v_k in G with $\Pi(v_0, v_k) \coloneqq \{\pi(v_0, v_k) \mid \pi(v_0, v_k) \subseteq G\}$.*

2.2. Electrical Engineering

This section is supposed to give a very brief introduction into the fundamental results from physics and electrical engineering that are used in this work.

A *direct current* (DC) circuit is a circuit consisting of sources of constant voltage and current as well as resistors. It is convenient to regard a circuit as an undirected graph $G = (V, E)$. The nodes V are the junction points, also called *buses* and the edges E are the connections between, laso called *branches*. It is the well-known equation $U = R \cdot I$ that describes the relation between the three properties voltage U, current I and resistance R. Furthermore, There are two fundamental laws every electrical circuit obeys, the so-called *Kirchhoff's circuit laws*:

1. *Kirchhoff's current law* (KCL): At every node of a circuit the sum of currents entering and leaving that point are zero:

$$\sum_{k}^{n} I_k = 0 \tag{2.4}$$

where n is the number of branches meeting at that bus. This is illustrated in Figure 2.1a.

2. *Kirchhoff's voltage law* (KVL): The sum of all voltages in a closed loop of circuit is zero:

$$\sum_{k}^{n} U_k = 0 \tag{2.5}$$

where n is the total number of voltages measured in a loop. This is illustrated in Figure 2.1b.

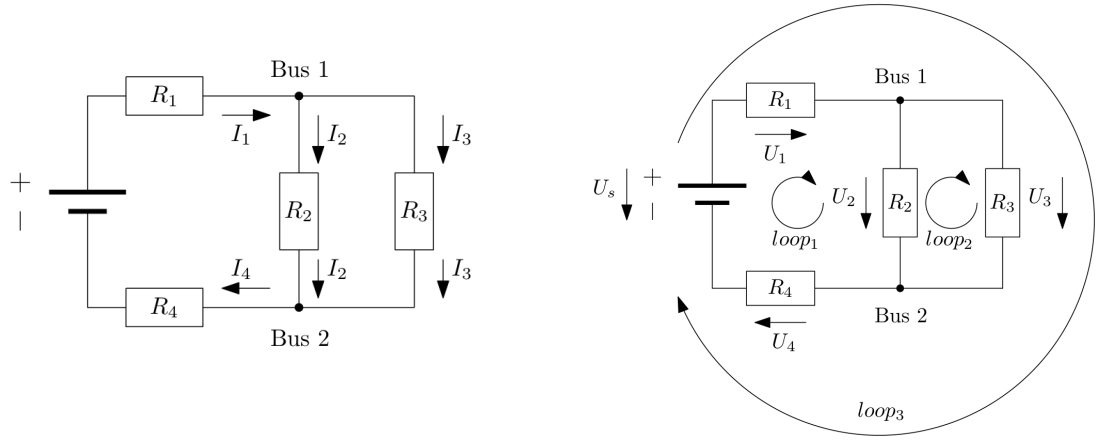

(a) KCL [Kru18]. Incoming currents equal the outgoing, i.e., $I_1 = I_2 + I_3$ (Bus 1) and $I_4 = I_2 + I_3$ (Bus 2).

(b) KVL [Kru18]. All voltages in a loop sum up to zero, e.g., $U_1 + U_2 + U_4 + U_s = 0$ ($loop_1$).

Figure 2.1.: Visualization of Kirchhoff's circuit laws.

In modern power grids the standard way to distribute energy is *alternating current* (AC). It is called alternating since the voltages and currents oscillate periodically, due to the way power is typically produced and transmitted. The following equations describe the *current* and *voltage* at a node in an AC circuit:

Definition 2.9 (Alternating Current & Voltage)**.** *Let $t \in \mathbb{R}_{\geq 0}$ be a point in time. The values of the oscillations of alternating current and voltage at this time are then given by the functions:*

$$i(t) = \hat{I} \cdot \cos(\omega t + \theta_i) \tag{2.6}$$

$$u(t) = \hat{U} \cdot \cos(\omega t + \theta_u) \tag{2.7}$$

where $\hat{I}$ ($\hat{U}$) is the amplitude of the oscillations, called peak current *(*peak voltage*). The* angular velocity $\omega = \frac{2\pi}{T}$ *represents the oscillations per second, with T denoting their period and 2π their wavelength. The shifts of the oscillations are given by $\theta_i, \theta_u \in [0, 2\pi)$ and called* phase angles.

Figure 2.2 illustrates the oscillations with all mentioned parameters. The assumption here is that we are dealing with perfect curves, which may be slightly off in the real world for

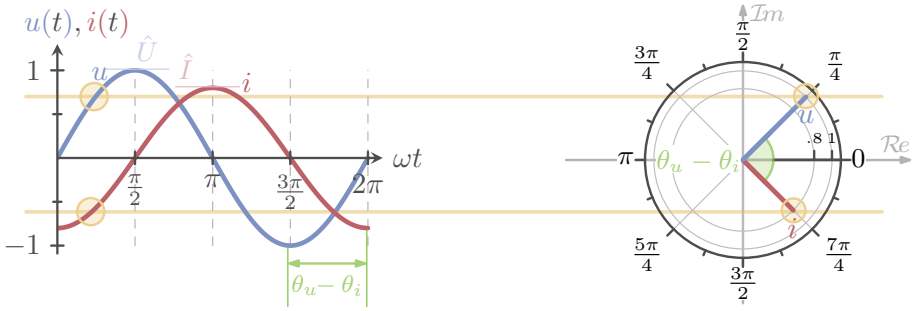

Figure 2.2.: Alternating current [Weg19]. The phase diagram (left) shows how voltage (u), current (i) and apparent power (s) oscillate over time and their representation in the complex plane (right).

technical and physical reasons. The *frequency* of AC is given by $f = \frac{2\pi}{T}$ with the unit being $\frac{1}{\text{s}} = 1\text{Hz}$.

Note that from now on we omit the time parameter in these terms, if it is not needed for disambiguation in order to increase readability. It is often convenient to express AC in terms of complex values. The oscillations of current and voltage can then be interpreted as rotating vectors around the origin of the complex plane, see Figure 2.2.

2.2.1. Power Grids

In a certain sense a power grid can be viewed as a large-scale electronic circuit with electrical components and wires connecting them. It consists of three essential building blocks:

- *Branches* represent the transmission lines that connect the other components.
- *Buses* bundle the ends of multiple branches as well as power generators and loads.
- *Transformers* are used to step the voltage up or down between subnetworks of different voltage levels.

Figure 2.3 shows an example diagram for a power grid consisting of 14 buses.

In an electric power grid the frequency of the oscillations of AC transmitted between the power stations and the end users are given by the *utility frequency*. The most widespread values for this are 60 and 50 Hz. The latter is also used in the European mainland power grid and is what we take in this work. Sticking to this frequency with only small deviations is imperative for a safe operation. A value undercutting the utility frequency means that the power demand is greater than the supply. Values exceeding it on the other hand imply an oversupply in produced power. Table 2.1 shows the measures taken in order to compensate for a frequency drop in the German power grid. Already a deviation of -0.2 Hz requires compensating actions and already at -2.5 Hz off the utility frequency the complete operation of the power grid comes to a halt in order to prevent major damage.

In the field of power engineering it is common practice to use the *per-unit* system which unifies the used units with regards to a reference value. Every quantity is converted to a per-unit quantity by dividing its actual value by the base value of the same dimension. This allows for the direct comparison of relevant electric parameters

Definition 2.10 (Per-unit Value)**.** *A* per-unit value *is a dimensionless value relative to a base value given by the following formula:*

$$\textit{per-unit quantity} = \frac{\textit{actual quantity}}{\textit{base value of quantity}} \tag{2.8}$$

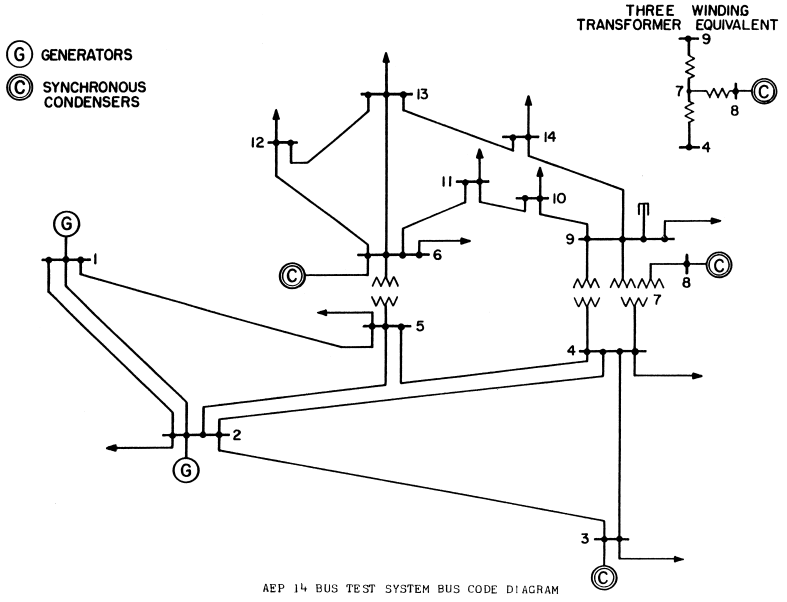

Figure 2.3.: Diagram for the IEEE 14-bus test case [AR15], representing a portion of the American electric power system. The thick horizontal numbered lines are buses. The circles labeled with G represent generators and the ones with C synchronous condensers. A load at a bus is depicted by an arrow, note that generators and loads can be connected to a bus simultaneously. The lines connecting the buses represent the branches.

Stage	**Frequency**	**Compensation / Safety Action**
1	49.8 Hz	Use of operating reserve
2	49.0 Hz	Immediate drop of $10 - 15\%$ of net load
3	48.7 Hz	Immediate drop of additional $10 - 15\%$ of net load
4	48.4 Hz	Immediate drop of additional $15 - 20\%$ of net load
5	47.5 Hz	Disconnect all power plants from the net

Table 2.1.: Safety measures in the German power grid to compensate for under frequency according to the *TransmissionCode 2007* [H$^+$07].

where the actual and the base quantity are of the same unit.

The procedure is then to pick two base values arbitrarily and derive the others from them. These are usually $U_{base} \in \{100\text{kV}, 400\text{kV}\}$, the base voltage and $P_{base} \in \{1\text{MVA}, 1000\text{MVA}, 1\text{GVA}\}$, the base power where the sets denote values commonly chosen. For the derivation of, for example, the base current we then calculate: $I_{base} = \frac{P_{base}}{U_{base}}$.

2.2.2. Power-Flow Equations

Next, we present how to model the power transmission in a power grid. The basic relation between voltage and current in a circuit is given by Ohm's law. In the case of AC this gives the following two important complex values:

Definition 2.11 (Impedance)**.** *The resistive value of an element in an AC circuit is called* impedance*, denoted by $\underline{Z}$. It is the ratio between voltage and current and:*

$$\underline{Z} = \frac{U}{I} = R + j \cdot X \tag{2.9}$$

where $R = Re(Z)$ is the electrical resistance *and $X = Im(Z)$ the electrical* reactance*.*

Definition 2.12 (Admittance)**.** *The* admittance $\underline{Y}$ *is defined as the reciprocal of impedance:*

$$\underline{Y} = \frac{1}{\underline{Z}} = \frac{R}{R^2 + X^2} + j \cdot \frac{-X}{R^2 + X^2} = G + j \cdot B \tag{2.10}$$

where $G = Re(Y)$ is the electrical conductance *and $B = Im(Y)$ the electrical* susceptance*.*

Admittance, as the inverse to impedance is a measure to express how easily load can pass through a conducting material. These are the values usually used to model the transmission lines of a power grid and hence are known as *line parameters*.

We model the branches by means of an RLC circuit where RLC stands for: resistor (R), inductor (L) and capacitor (C). Such a model of the transmission lines is according to [SR70] and called Π-*equivalent model*. Figure 2.4 shows a Π-equivalent representation of a transmission line. The name resembles the structure of the circuit.

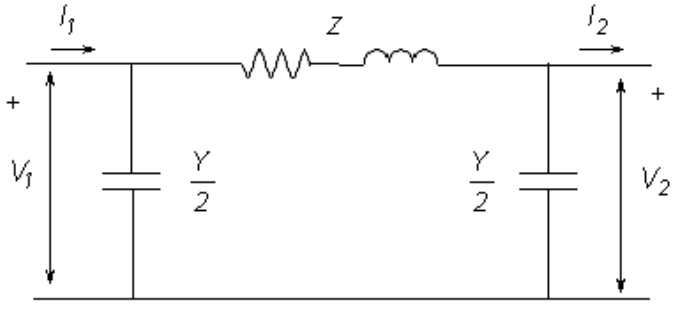

Figure 2.4.: Representation of a transmission line using a Π-equivalent circuit [pi-]. V_1 and I_1 are the voltage and current at the sending end, V_2 and I_2 at the receiving end respectively. Y is the shunt admittance and Z the impedance.

We now want to look at the electrical power in AC circuits, the *complex power* is defined as follows:

Definition 2.13 (Complex Power)**.** *The* complex power $\underline{S}$ *in an AC circuit is given by:*

$$\underline{S} = P + j \cdot Q \tag{2.11}$$

, where $j = \sqrt{-1}$ *denotes the complex unit. We call* $P = Re(\underline{S})$ real power *and* $Q = Im(\underline{S})$ reactive power*.*

The imaginary reactive power is temporarily stored in capacities or inductances. This effect arises because of the induced currents from the AC oscillating in the transmission lines.

With this we can finally introduce the equations that are referred to as *AC load-flow* equations [GSO12]. They describe how much power is produced or consumed at one node with regard towards the other nodes in the network.

Definition 2.14 (Load-Flow Equations)**.** *Consider a power grid with* n *buses. The injected real and reactive power at bus* $i = 1, ..., n$ *are:*

$$P_i = \hat{U}_i \sum_{k=1}^{n} \hat{U}_k (G_{ki} \cos(\theta_k - \theta_i) + B_{ki} \sin(\theta_k - \theta_i)) \tag{2.12}$$

$$Q_i = \hat{U}_i \sum_{k=1}^{n} \hat{U}_k (G_{ki} \sin(\theta_k - \theta_i) - B_{ki} \cos(\theta_k - \theta_i)) \tag{2.13}$$

where $\hat{U}_i$ *is the maximum voltage at bus* i*,* G_{ki} *is the conductance on the branch connecting bus* k *with* i*,* B_{ki} *is its susceptance and* $\theta_k - \theta_i$ *is the voltage angle difference between buses* k *and* i*.*

2.3. Ordinary Differential Equations

In mathematics, a phenomenon which evolves with time in a way such that only the present affects the future is called a *dynamical system.* The behavior of such a system is expressed in the terms of *differential equations.* As the system function (usually called y) is often unknown, a differential equation describes this function with the function‘s values and the ones of its derivatives.

A special case are so-called *ordinary differential equations* (ODEs) in which the searched function and its derivatives contain only one independent variable. Most commonly, as also in this work, the independent variable is the time and is hence denoted by t.

Definition 2.15 (Ordinary Differential Equation)**.** *Let* $D \subseteq \mathbb{R} \times \mathbb{R}^n, n \in \mathbb{N}$ *and* $f : D \to \mathbb{R}$ *a continuous function. We call*

$$f\left(t, y(t), y'(t), \ldots, y^{(n)}(t)\right) = 0$$

an ordinary differential equation of order n*, where* $(y', y'', \ldots, y^{(n)})$ *is Lagrange's notation to depict the i-th derivative, i.e.,* $y^{(i)} = \frac{d^i y}{dx^i}$*.*

The value $y(t)$ is called the state of the system at time t. In the above definition the ODE is in so-called *implicit form.* If the ODE is solved for the highest derivative on one side, i.e., $f\left(t, y(t), y'(t), \ldots, y^{(n-1)}(t)\right) = y^{(n)}(t)$ we call it *explicit.*

For some ODEs the development of states is not depending on the time but only on the previous state the system was in. Then we can omit t as a parameter and the only time-dependent variables are the ones represented by $y(t)$ and its derivatives. We call such an ODE *autonomous.*

Definition 2.16 (Autonomous Ordinary Differential Equation)**.** *An ordinary differential equation* $f\left(t, y(t), y'(t), \ldots, y^{(n-1)}(t)\right) = y^{(n)}(t)$ *is called* autonomous*, if*

$$f\left(y(t), y'(t), \ldots, y^{(n-1)}(t)\right) = y^{(n)}(t)$$

for all t *in the function domain.*

For this work we are only interested in autonomous ODEs and hence consider only these from now on.

More complex phenomena are described not only by one ODE but by several coupled equations. Together they form a *system* of ordinary differential equations.

Definition 2.17 (System of Ordinary Differential Equations)**.** *Let* $\boldsymbol{y}$ *be a vector whose elements are functions* $\boldsymbol{y} = (y_1(t), y_2(t), \ldots, y_m(t))$*,* $m \in \mathbb{N}$ *and* $\boldsymbol{f} : (\mathbb{R}^m)^n \to \mathbb{R}^m$ *a vector-valued function of* $\boldsymbol{y}$ *and its derivatives then*

$$\boldsymbol{y}^{(n)} = \boldsymbol{f}\left(\boldsymbol{y}, \boldsymbol{y}' \ldots \boldsymbol{y}^{(n-1)}\right)$$

is a system of ODEs with order n and dimension m*. In column vector form:*

$$\begin{pmatrix} y_1^{(n)}(t) \\ y_2^{(n)}(t) \\ \vdots \\ y_m^{(n)}(t) \end{pmatrix} = \begin{pmatrix} f_1(\boldsymbol{y}, \boldsymbol{y}', \ldots, \boldsymbol{y}^{(n-1)}) \\ f_2(\boldsymbol{y}, \boldsymbol{y}', \ldots, \boldsymbol{y}^{(n-1)}) \\ \vdots \\ f_m(\boldsymbol{y}, \boldsymbol{y}', \ldots, \boldsymbol{y}^{(n-1)}) \end{pmatrix}.$$

A system of autonomous differential equations is also called *autonomous system.*

When it comes to performing computations with autonomous ODEs it is convenient to only look at systems of first order. We reduce an equation of order n by introducing n new independent functions $y_i(t) = y^{(i)}(t)$, $i = 1, 2, \ldots, n$:

$$\begin{aligned} y_0(t) &= y(t) \\ y_1(t) &= y'(t) = \frac{dy_0}{dt} \\ y_2(t) &= y''(t) = \frac{dy_1}{dt} \\ &\ldots \\ y_{n-1}(t) &= y^{(n-1)}(t) = \frac{dy_{n-1}}{dt} \\ y_n(t) &= f(y_0, y_1, \ldots, y_{n-1}) \end{aligned}$$

So each consecutive function is a first order derivation of the introduced equation before. With this we get a system of $n \cdot m$ equations when we reduce a system of m equations of order n.

It often is very hard or even infeasible to find analytical solutions for differential equations. However, in many cases it suffices to study a system in its *fixed points* in order to be able to make qualitative statements about the behavior. At such points the system is time-invariant, i.e. does not change its behavior in the future.

Definition 2.18 (Equilibrium Point)**.** *Let* $\boldsymbol{f}\left(\boldsymbol{y}, \boldsymbol{y}' \dots \boldsymbol{y}^{(n-1)}\right) = \boldsymbol{y}^{(n)}$ *be an autonomous system of order* n*. A point* $\boldsymbol{y^e} \in \mathbb{R}^n$ *that solves the system is called a* equilibrium point*, if*

$$\boldsymbol{f}\left(\boldsymbol{y}^e\right) = 0$$

Equilibrium points are also known as *fixed points*. Note that in this point all derivatives $\boldsymbol{y}', \boldsymbol{y}'', \dots$ become zero.

For the analysis of dynamical systems we are interested in how they behave close to an equilibrium point. An equilibrium is called *stable* if a system's states that lie in an area with small distance ϵ around an equilibrium will never develop out of this area. Whereas an equilibrium is called *unstable*, if the system's states develop away from it and sometimes behave in unwanted ways.

Definition 2.19 (Stability of an Equilibrium Point)**.** *An equilibrium point* $\boldsymbol{y}^e$ *is called* stable*, if for every* $\epsilon > 0$ *there exists a* $\delta > 0$ *s.t. for every solution* $\boldsymbol{f}(\boldsymbol{y}(t))$ *having initial conditions within distance* δ*, i.e.,* $\|\boldsymbol{f}(\boldsymbol{y}(t_0)) - \boldsymbol{f}(\boldsymbol{y}^e)\| < \delta$ *remains within distance* ϵ*, i.e.,* $\|\boldsymbol{f}(\boldsymbol{y}(t)) - \boldsymbol{f}(\boldsymbol{y}^e)\| < \epsilon$ *for all* $t \geq t_0$*.*

For the assessment of the stability of equilibrium points we will need to calculate eigenvalues which are defined as follows.

Definition 2.20 (Eigenvector, Eigenvalue)**.** *Let* V *be a vector space over a field* K *and* $f : V \to V$ *a linear transformation from* V *into itself. We call* $\boldsymbol{v} \in V, \boldsymbol{v} \neq \boldsymbol{0}$ *an* eigenvector*, if* $f(\boldsymbol{v})$ *is a scalar multiple of* $\boldsymbol{v}$*, i.e.,*

$$f(\boldsymbol{v}) = \lambda \boldsymbol{v}$$

where $\lambda \in K$*. We call* λ *the* eigenvalue *associated with* $\boldsymbol{v}$*.*

As there is a direct correspondence between square matrices and linear transformations the above definition can be as $\boldsymbol{A}\boldsymbol{v} = \lambda \boldsymbol{v}$ where $\boldsymbol{A}$ is the matrix representation of f.

3. The DC Model

In this chapter we introduce a graph-theoretic representation of the power grid that can be used to optimize the power flow based on topological properties. One of the simplest ways to model electrical power grids is the so-called *DC model* which is a linear approximation of the nonlinear AC load-flow equations we saw in Definition 2.14. The resulting model shows similar properties to the behavior of direct current which is why it is referred to as DC model. Its derivation is based on three central assumptions, as presented in [ZMsT+11].

3.1. Derivation

As this work focuses on state- or countrywide high and highest voltage networks, the coarseness and high voltage levels at these layers of the power grid allow for some convenient simplifications. The established model relies on the following important assumptions in order to be computationally more tractable.

A1 Negligible line resistance. We assume the transmission line resistance R to be very small, compared to the reactance X i.e., $R \ll X$ for all lines. This means we ignore ohmic losses and consequently set $R = 0$. The justification for this is that with increasing voltage levels the resistances are getting quadratically smaller. With Definition 2.12 this simplifies the parameters

$$G_{ij} = \frac{R_{ij}}{R_{ij}^2 + X_{ij}^2} = 0$$
$$B_{ij} = \frac{-X_{ij}}{R_{ij}^2 + X_{ij}^2} = -\frac{1}{X_{ij}}$$

Hence, the admittance in the DC model is purely imaginary and the power flow equations become:

$$P_i = \hat{U}_i \sum_{k=1}^{n} \hat{U}_k \cdot B_{ik} \sin(\theta_k - \theta_i)$$
$$Q_i = \hat{U}_i \sum_{k=1}^{n} \hat{U}_k \cdot B_{ik} \cos(\theta_k - \theta_i)$$

A2 Flat voltage profile. The voltage profiles are assumed to be flat at each node. This means the voltage magnitudes are usually set to the reference voltage level: $\hat{U}_i = 1.0\ p.u.$ for all buses i. The load-flow equations therefore simplify further to:

$$P_i = \sum_{k=1}^{n} B_{ik} \sin(\theta_k - \theta_i)$$
$$Q_i = \sum_{k=1}^{n} B_{ik} \cos(\theta_k - \theta_i)$$

A3 Negligible voltage angle differences. In power grids voltage angle differences are usually rather small. In [PMVB05] the authors found that for the Belgian high voltage network most of the observed angle differences are below $2°$, while the peak values are at around $6° - 7°$. Therefore, using the angle differences directly is feasible and results in the following approximation:

$$\sin(\theta_j - \theta_i) \approx \theta_j - \theta_i$$
$$\cos(\theta_j - \theta_i) \approx 1$$

Note that the slope of the sine function around the origin is close to linear while that of the cosine is almost flat. This leads to the approximations with a linear term and constant 1 respectively. With this, we can omit the reactive power equations and the power flow equations finally reduce to:

$$P_i = \sum_{k=1}^{n} B_{ik}(\theta_k - \theta_i) \tag{3.1}$$

We have reduced the nonlinear, non-convex problem formulation of the AC power flow to a system of linear equations. With these we now can introduce a power grid model based on a flow network.

3.2. Graph-Theoretic Representation

Every power grid can be described as a connected, undirected graph $G = (V, E)$. Figure 3.1a shows the example power grid of Section 2.2. Figure 3.1b shows the corresponding graph to it. The branches and branch related equipment such as transformers are now represented by the edges E, where one edge represents all the lines between two buses combined. The set of nodes V corresponds to the buses. We partition them into two disjoint subsets $V = V_G \dot{\cup} V_C$, where V_G represents the generators and V_C the consumers connected to the grid. Note that a bus can be connected to generators and loads simultaneously (e.g. bus 2). We consider the corresponding node to be a generator if the real power injected exceeds the amount of load at this bus, $P_i > 0$ and to be a consumer if $P_i \leq 0$. Transformers (bus 7) are neither of the above and are implicitly represented by edges and other network parameters.

In order to capture DC power flows as derived in the previous section we take the graph representation of a power grid and then define a flow network as in Definitions 2.5 and 2.6 with additional properties to capture the physical world we are talking about. Following [GRW+18], a graph-theoretic representation of a power grid can be defined as follows: The sources of the network correspond to the generators V_G of the power grid and the sinks to the loads V_C. The capacity function *cap* represents the *thermal line limits* of the transmission

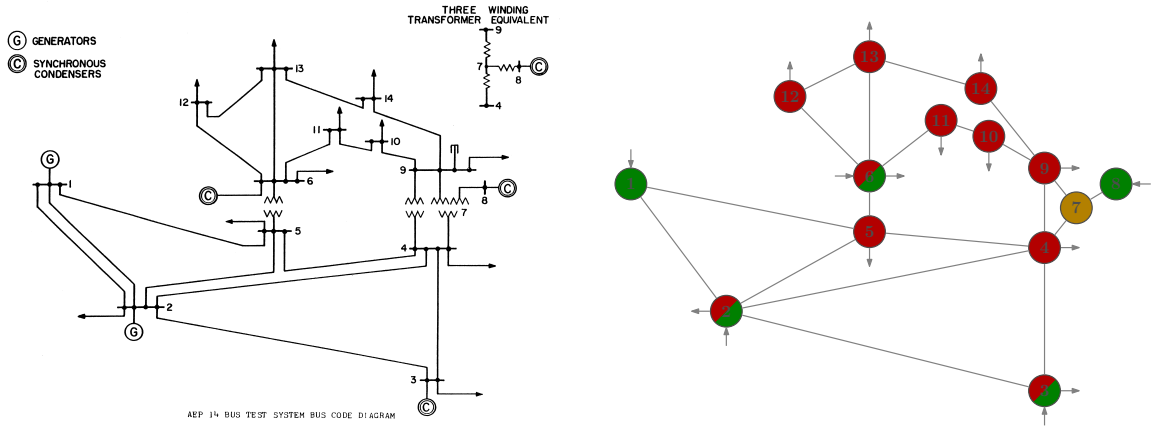

(a) Power grid diagram [AR15]. (b) Graph representation.

Figure 3.1.: The IEEE 14-Bus system diagram and its corresponding graph. Generators G and Condensers C become V_G (■), outgoing arrows indicating loads become V_C ■. Transformers (■) are implicitly modeled by the edges and only shown for completeness.

lines. This constraint is introduced to make the upcoming optimization problems well-defined by limiting the flows. Beyond the capacity we also define a susceptance function b mapping the line parameter to each of the edges. The minimal demand of the load nodes is given by function $\underline{p_d}$, the maximum by $\overline{p_d}$ and the lower and upper bounds for the power a generator node can provide are given by $\underline{p_g}$ and $\overline{p_g}$.

Definition 3.1 (DC Network [GRW+18])**.** *Let $\vec{G} = (V, \vec{E})$ be a bi-directed graph. The DC network, representing a power grid, is then given by the tuple $\mathcal{N} = (\vec{G}, V_G, V_C, cap, b, \underline{p_d}, \overline{p_d}, \underline{p_g}, \overline{p_g})$ with:*

$$
\begin{aligned}
V_G &\subseteq V && \text{generator nodes}\\
V_C &\subseteq V && \text{consumer nodes}\\
cap &: \vec{E} \to \mathbb{R}_{\geq 0} && \text{capacity function}\\
b &: \vec{E} \to \mathbb{R}_{\geq 0} && \text{susceptance function}\\
\underline{p_d} &: V_C \to \mathbb{R}_{\geq 0} && \text{consumer's minimum demand}\\
\overline{p_d} &: V_C \to \mathbb{R}_{\geq 0} && \text{consumer's maximum demand}\\
\underline{p_g} &: V_G \to \mathbb{R}_{\geq 0} && \text{generation's lower bound}\\
\overline{p_g} &: V_G \to \mathbb{R}_{\geq 0} && \text{generation's upper bound}
\end{aligned}
$$

Given a DC network $\mathcal{N}$, a flow on this network is a function $f : \vec{E} \to \mathbb{R}$ satisfying the conditions of Definition 2.6. We furthermore define the *net flow* at a node in Definition 3.2.

Definition 3.2 (Net Flow [GRW+18])**.** *Let $\mathcal{N} = (\vec{G}, V_G, V_C, cap, b, \underline{p_d}, \overline{p_d}, \underline{p_g}, \overline{p_g})$ be a DC network with $\vec{G} = (V, \vec{E})$ and $f : \vec{E} \to \mathbb{R}$ a flow. The net flow at a node $v \in V$ is defined as*

$$f_{net}(v) \coloneqq \sum_{(v,w)\in\vec{E}} f(v, w) \tag{3.2}$$

It has to satisfy the following three constraints:

$$f_{net}(v) = 0 \qquad \forall v \in V \setminus (V_G \cup V_C) \tag{3.3}$$

$$-\infty \leq f_{net}(v) \leq -\underline{p_d}(v) \qquad \forall v \in V_C \tag{3.4}$$

$$\underline{p_g}(v) \leq f_{net}(v) \leq \overline{p_g}(v) \qquad \forall v \in V_G \tag{3.5}$$

Equation (3.3) resembles Kirchhoff's current law (see Equation (2.4)) that itself is equivalent to the flow conservation in Equation (2.2). In these cases Equation (3.4) constraints the net flow with the demands lower limit at a consumer node and Equation (3.5) limits the net flow with the generation bounds.

The *flow value* F of a flow f on network $\mathcal{N}$ is given by the total amount of units of flow injected by the generator nodes into the network, see Equation (3.6).

$$F(f,\mathcal{N}) \coloneqq \sum_{v \in V_G} f_{net}(v) \tag{3.6}$$

The maximal achievable flow value for a feasible flow defined on a network $\mathcal{N}$ is called Maximum Flow (MF) and is defined as follows:

Definition 3.3 (Maximum Flow)**.** *Let $\mathcal{N}$ be a DC network with $\vec{G} = (V, \vec{E})$. A feasible flow $f : \vec{E} \to \mathbb{R}_{\geq 0}$ is called* Maximum Flow *(MF) if*

$$f = \arg\max_{f} F(f,\mathcal{N}). \tag{3.7}$$

Its value is given by $OPT_{MF}(\mathcal{N}) \coloneqq \max F(f,\mathcal{N})$.

So far the definitions mostly correspond to the ones of a classical network flow model. Now, additionally we want to be able to represent the physical properties of electrical grids. More precisely, we aim to express the linearized power flow of Section 3.1 in graph-theoretic notation.
First, we define a function $\Theta : V \to \mathbb{R}$ mapping a *potential* value to each bus. In an electric grid the difference in voltage angles between two buses is proportional to the amount of power that can be transmitted over a line at once. Note that Equation (2.3) already puts an upper bound to this difference in constraining how much flow actually can be transmitted. The other property that influences how much power can flow through a branch is given by the susceptance b. An *electrically feasible* flow has to satisfy the conditions given in Definition 3.4.

Definition 3.4 (Electrical Feasibility)**.**

$$b(v,w) \cdot (\Theta(w) - \Theta(v)) = f(v,w) \qquad \forall (v,w) \in \vec{E} \tag{3.8}$$

$$\Theta_{min}(v) \leq \Theta(v) \leq \Theta_{max}(v) \qquad \forall v \in V \tag{3.9}$$

Equation (3.8) resembles the linearization assumptions of Section 3.1. We see that the higher the susceptance, the more power can flow between two potentials. This equation, together with Equation (2.2), also implicitly models the KVL. Nodes in any cycle in a graph have to be assigned with voltage levels such that summed up they become zero. Equation (3.9) gives a limitation to the maximum phase angles and hence also to the maximum phase angle difference $\Theta(u) - \Theta(v)$ between two adjacent nodes. Values from the NESTA dataset suggest $\Theta_{min} = -30°$ and $\Theta_{max} = 30°$.
With this expansion of the model, giving an edge $(v,w) \in \vec{E}$ a positive flow value $f(v,w) > 0$ means power proportional to this value is transmitted from node v to node w. If $f(v,w) < 0$ the power is actually transmitted from w to v. We call a flow f that is electrically feasible a *power flow*.

Analogously to Definition 3.3, the electrically feasible power flow for a network $\mathcal{N}$ that maximizes $F(f,\mathcal{N})$ is called Maximum Power Flow (MPF) and its value is given by $\mathrm{OPT}_{MPF}(\mathcal{N}) \coloneqq \max F(f,\mathcal{N})$.

3.2.1. Switching

It can happen that the maximum power flow of a given DC network is limited by certain edges. In that case removing them can actually achieve a greater flow value. Figure 3.2 shows such a situation. The maximal possible power flow in Figure 3.2a is $\frac{3}{2}$, as edge (s,t) is saturated and the resulting potential of 1 at node t does not allow for more flow via node x. After removing edge (s,t) (Figure 3.2b) the flow increases to 2 with higher potentials possible at the nodes.

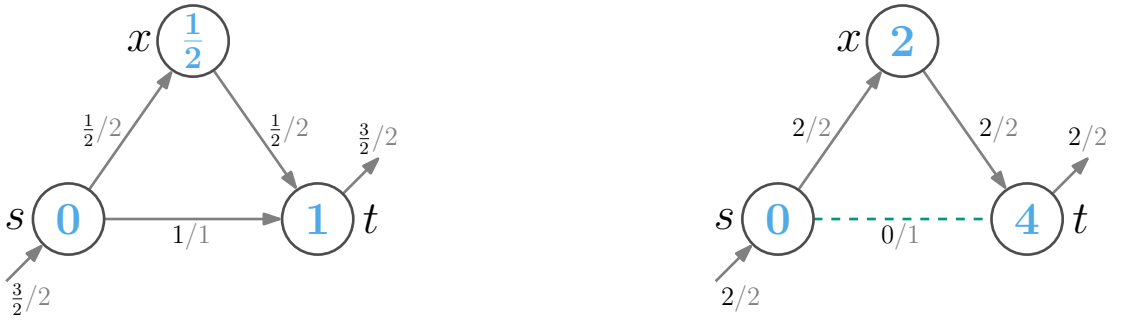

(a) Network without switching. $\mathrm{OPT}_{MPF}(\mathcal{N}) = \frac{3}{2}$

(b) Network after switching edge (s,t). $\mathrm{OPT}_{MTSF}(\mathcal{N}) = 2$

Figure 3.2.: Example for applied switching increasing the flow [Weg19]. All line susceptances are set to $b = 1$. The gray edge labels denote the capacity *cap*, the black labels the flow f. The blue numbers in the nodes give the potential Θ.

We now give a formal definition of switching. Let $G = (V, E)$ be an undirected graph and $S \subseteq E$ the set of edges we want to remove from G. We obtain $G - S := (V, E \setminus S)$. For the corresponding directed graph $\vec{G} = (V, \vec{E})$ define the set of removed edges as $\vec{S} := \{(v,w), (w,v) \mid \{v,w\} \in S\}$ and get $\vec{G} - \vec{S} := (V, \vec{E} \setminus \vec{S})$.
The DC network with switched-out edges S is then given by $\mathcal{N} - S := (\vec{G} - \vec{S}, V_G, V_C, cap', b', \underline{p_d}, \overline{p_d}, \underline{p_g}, \overline{p_g})$ where $b' : \vec{E} \setminus \vec{S} \to \mathbb{R}_{\geq 0}$ and $cap' : \vec{E} \setminus \vec{S} \to \mathbb{R}_{\geq 0}$ are the susceptance and capacity function restricted to the remaining edges.

Definition 3.5 (Maximum Transmission Switching Flow)**.** *Let $\mathcal{N}$ be a DC network. A* Maximum Transmission switching Flow *(MTSF) on $\mathcal{N}$ is given by*

$$MTSF(\mathcal{N}) := max_{S \subseteq E} MPF(\mathcal{N} - S) \tag{3.10}$$

Its value is given by $OPT_{MTSF}(\mathcal{N})$.

Note that this definition only regards electrically feasible flows.

The following lemma shows the relationship between the maximum flow values. A general MF without physical constraints is always the best we can achieve and gives an upper bound. An MTSF is always at least as good as an MPF, since we can just set $S = \emptyset$.

Lemma 3.6 ([GRW+18])**.** *Let $\mathcal{N}$ be a DC network. The following relations hold:*

$$OPT_{MPF}(\mathcal{N}) \leq OPT_{MTSF}(\mathcal{N}) \leq OPT_{MF}(\mathcal{N}).$$

Dominating Theta Paths

Now, in order to find edges that lead to optimal switchings we look at a new centrality measure introduced by the authors, the *dominating theta path* (DTP)-betweenness centrality. For this we need two more definitions. Paths $\pi(v, w)$ are defined as in Definition 2.7.
The *susceptance norm* for a path $\pi(v, w)$ in a DC network $\mathcal{N}$ is given by Equation (3.11):

$$\|\pi(v,w)\|_b \coloneqq \sum_{e\in\pi(v,w)} b(e)^{-1} \tag{3.11}$$

The *minimum capacity* on a path $\pi(v, w)$ is given by Equation (3.12).

$$\underline{\text{cap}}(\pi) \coloneqq \min_{(v,w)\in\pi} cap(u,w) \tag{3.12}$$

The potential difference on a path, i.e. between the start and the finish node can then be calculated as given in Definition 3.7.

Definition 3.7.

$$\Delta\Theta(\pi(v,w)) \coloneqq \|\pi(v,w)\|_b \cdot \underline{cap}(\pi(v,w)) \tag{3.13}$$

Let $\Pi(v, w)$ be the set of all paths from v to w in a given graph (Definition 2.8). A switching is assumed to be beneficial if it removes an edge sitting on a path that limits the maximum flow. Such a path is limiting, if it has the smallest the potential difference $\Delta\Theta\pi(v, w)$ of all v-w-paths. We call this path a dominating theta path.

Definition 3.8 (Dominating Theta Path [GRW$^+$18])**.** *The* Dominating Theta Path *(DTP) between two nodes v and w is given by:*

$$\pi_{DTP}(v,w) \coloneqq \underset{\pi(v,w)\in\Pi(v,w)}{\arg\min} \Delta\Theta(\pi(v,w)) \tag{3.14}$$

In [GRW$^+$18] the authors present an algorithm for finding DTPs in DC networks. For every pair of nodes (u, v) there exists such a DTP. The metric for the removal of an edge is now not, whether there is a DTP going through this edge, but how many. By looking at edges like this we receive a new centrality measure that is not based on shortest paths but rather following the intuition of the 'path of least resistance'.

Definition 3.9 (DTP Betweenness Centrality [GRW$^+$18])**.** *Let $\mathcal{N}$ be a DC network. The* DTP betweenness centrality *$c_{DTPB} : E \to \mathbb{R}_{\geq 0}$ is given by*

$$c_{DTPB}(e) \coloneqq \frac{1}{m_B} \sum_{s\in V} \sum_{t\in V\setminus\{s\}} \frac{\sigma_{DTP}(s,t,e)}{\sigma_{DTP}(s,t)} \tag{3.15}$$

where $\sigma_{DTP}(s, t, e)$ is the number of DTP-paths between s and t that use e, $\sigma_{DTP}(s, t)$ is the total number of DTP-paths from s to t and $m_B = |V|(|V| - 1)$ is a normalizing constant.

With the normalization constant m_B we get $c_{\text{DTPB}}(e) \in [0, 1]$ for all edges. Where a higher values implies e is element of more DTP-paths.

3.3. Limitations of the Model

As it was shown in [LGV14, LGHV15] finding the MTSF in general is NP-hard and only for certain rather limited graph classes better results on the problem complexity are known. For general graphs it was even shown that there exists no effective approximation algorithm to solve the switching problem. Yet, in [GRW+18] the authors present an algorithm that computes the dominating theta paths of which is not known whether it runs in polynomial time, but shows reasonable running times and results on realistic problem instances.

They also show that their algorithm computes a correct MTSF for a specific graph class, so-called penrose-minor-free graphs with only one generator and one consumer. Beyond that there are only simulation results for more general graphs, e.g. of the NESTA dataset, so far. The suggestion hence is to use the DTP-betweenness definition from above as a heuristic for finding edges most likely to be congested and therefore being the best candidates to remove in order to increase the overall power flow.

While we can use the DTP-betweenness as an indicator for how beneficial a switching may be, even though in most cases only heuristically, up to now we have no evidence whether the removal of the computed edges will actually leave us with an intact power grid. This is because the performed analysis is static. We only look at a snapshot of the power grid at one point in time with the corresponding load, generation and phase angles. We compute the switchings and optimize flow values based on this state. So far, there is no way to express how the power grid is going to behave over time, after we perform such a big intervention as topologically altering it. The result is a relocation of load on the network edges which will also alter the phase angles of the generators and loads as well as the net frequency.

However, as mentioned in Section 2.2, deviations from the utility frequency of 50Hz that are too large can cause severe damage and leave the power grid inoperable. We therefore want to be able to analyze what happens at the different buses after a switching took place. Also, such potentially disruptive events all happen on a rather small time scale, as power transmission is fast and effects can take place quickly at different nodes over the whole net.

We also have to keep in mind that we are looking at a linearized model of the power grid. There are possible sources for errors as investigated and presented in [PMVB05]. The lower the voltage levels are the more likely it is that Assumption **A1** (negligible line resistance) and Assumption **A3** (small voltage angle differences) can cause errors. Assumption **A2** (flat voltage profiles) appears to be the most critical one as the nodal voltages are distributed around 1.1 p.u. rather than 1 p.u. which causes the most estimation error. A reason for this higher value is to account for voltage drops along transmission lines.

In conclusion, we do not know if the heuristics on the DC network with all the simplifications mentioned can be applied to compute switchings just like that or if they would desynchronize and destroy the represented power grid. We hence need to look at another model which takes into account a notion of time in order to be able to perform a transient analysis and to assess the stability.

4. Dynamic Modeling

With the static DC model at hand and the concerns about the stability of the power grid we now derive a different modeling approach that incorporates an element of time. The aim is to study dynamic events and their consequences such as the switching of an edge but also change in supplied or demanded power at a generator or consumer node. A redistribution of the power flow consequently leads to a change in the voltage angles at the buses and a change of the net frequency is the result. How big is the impact of these shifts in the flow over the edges? What influence does it have on the system's stability? This can only be observed over a period of time.

In a power grid the net frequency is determined by the rotations of the generators' turbines. It gives very sensitive responses to scenarios such as oversupply or overload. In ideal conditions every unit is running exactly with the utility frequency which in our case is 50 Hz. In practice, however, the frequency of the grid varies. It reduces when the net is heavily loaded, i.e., the demand is greater than the supply and increases when there is more supply than demand, see Section 2.2.1. Roughly speaking, if there is more energy in the system the frequency increases. An analogy for this is radiation: higher energetic waves such as gamma radiation have a higher frequency. Hence, the goal is to keep the machines of the grid overall as close as possible to the desired reference of 50 Hz.

The key condition for proper operation in which we are interested in this chapter is the *synchronization* of the frequencies of all the interconnected machines. Although we want to shed light onto this more detailed aspect, we still want to have a model that is feasible for a network on the same scale as the linear DC model. This means high voltage nationwide transmission networks. We do not want to worry about too specific technical details of every component. The *oscillator model* grants exactly this compromise between large scale topological considerations and dynamical behavior.

4.1. The Oscillator Model

The formalization of synchronization behavior was originally introduced by Kuramoto [Kur75] in 1975. It defines a system of ordinary differnetial equations of first oder. The idea is that periodical behavior of some entity can affect the behavior of neighboring ones such as for example neural cells. The entities are modeled as oscillators that are coupled with each other via some kind of connection that affects the rotations of the oscillators mutually. When the coupling is strong enough and the differences between

the oscillators rotations is not too large they will eventually synchronize to operate at the same frequency. Originally, this model was only defined on complete graphs with homogeneous coupling values. However, as real world systems are often heterogeneous and exhibit complex structural properties, it has been extended to complex networks, with also additional features such as time-delay in the interactions [RPJK16].

This concept of coupled oscillators was first utilized for power grid analysis by Filatrella et al. [FNP08] in 2008. The connection is clear as AC oscillates periodically in the power grid and generator turbines and electric motors are rotating machines that have to be operated at the same frequency. We now derive the model to express these nonlinear dynamics on small time scales. This is will give us insight into the dynamic behavior that happens as a response to the switching operations we with to study. The model consists of a set of ordinary differential equations, one for each bus of the network.
Much like the static DC model it is based on some simplifying assumptions we can make when we look at the high voltage transmission network. We can then simplify the power flow equations from Definition 2.14 by the following assumptions:

- The model is lossless, i.e., we ignore ohmic losses among the transmission lines (see assumption **A1**).
- The nodes' voltage amplitudes are constant across all nodes and time, i.e. $\hat{U}_i(t) = 1$ p.u. for all $i \in V$ (see assumption **A2**).
- We only consider active power transmission.

This time however the voltage angle differences are not negligible and we do not linearize the model. Applying these assumptions leads us to Equation (4.1).

$$P_i = \sum_{j=1}^{N} B_{ij} \sin(\theta_j - \theta_i) \tag{4.1}$$

In comparison to the load flow equation of the DC model, Equation (3.1), we now have a power flow that is equivalent to the sine of the phase angle differences $\theta_j - \theta_i$.

Again, as in Section 3.2, we represent a power grid with an undirected graph $G = (V, E)$ with a set of buses V and branches E, representing the topology of the power grid. Note that this time we make no distinction between generator and consumer nodes. The oscillator model thinks of each node in the network as a rotating machine such as a power generating turbine or power consuming motor. These machines are coupled with each other by the transmission lines between them. Generators in this net aim to produce power that is close to the utility frequency. Since we are in a rotating frame we set the network's *reference angular frequency* to

$$\Omega \coloneqq 2\pi \cdot 50 \text{ Hz}$$

which describes the angular change. Here these are 50 rotations per second.

Every machine $i \in V$ has a *state* that is described by two values. Again, for the sake of readability after its definition we omit a function's time parameter if it is not needed for disambiguation and write f instead of $f(t)$.

1. The *mechanical phase angle* $\theta_i(t)$ at time $t \in \mathbb{R}_{\geq 0}$ for machine i is given by Equation (4.2).

$$\theta_i(t) = \Omega t + \phi_i(t) \tag{4.2}$$

   Function $\phi_i(t)$ denotes the *phase shift* from the reference phase Ωt.

2. The *angular velocity* represents the angle change of machine i oder time t and is given by Equation (4.3).

$$\frac{d\theta_i(t)}{dt} = \dot{\theta}_i(t) = \Omega + \dot{\phi}_i(t) \tag{4.3}$$

This is the first derivative of the angle function and also known as the oscillator's frequency. Note that from now on we use Newton's notation for derivatives, i.e, $\dot{\theta}, \ddot{\theta}$ as it is habit in physics when calculating with time derivatives. As we saw in Section 2.2.1 only small deviations from the utility frequency are allowed in AC power grids. An important assumption is therefore that the phase changes are small compared to the reference angular frequency: $|\dot{\phi}_i| \ll \Omega$.

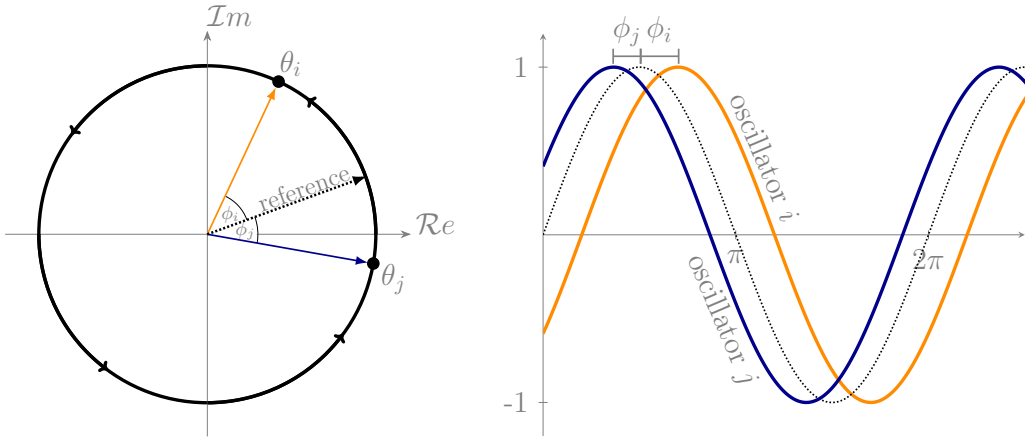

Figure 4.1.: Illustration of two oscillators i (■) and j (■) wrt. the reference oscillation. On the left the oscillations are represented as rotations on the unit circle in the complex plane. Angles ϕ_i and ϕ_j give the phase shift from the reference (dashed). The phase development over time is given. It shows how oscillator i is ahead by ϕ_i and oscillator j is behind by ϕ_j while the frequencies $\dot{\phi}_i$, $\dot{\phi}_j$ is the same.

In order for power transmission to take place between two nodes $i, j \in V$ it is required that they do not operate in phase. In Equation (4.1) we saw that the transmitted power is proportional to the sine of the voltage angle difference. Since $\sin(\theta_j - \theta_i) = 0$, if $\theta_j = \theta_i$ the phase angles have to differ. As all pairs (i, j) of oscillators have the same reference frequency, their differences in phase angles and phase deviations are the same: $\theta_{ij} = \theta_i - \theta_j = \phi_i - \phi_j = \phi_{ij}$.

Figure 4.1 shows how the oscillations can be thought of as rotations as well as waves. Now, if a node i is connected to j and is 'ahead' with its phase angle, i.e. $\theta_i(t) > \theta_j(t)$, power is transmitted from i to j, as $\sin(\theta_i(t) - \theta_j(t)) > 0$. This means, if i is a generator and starts to produce more power at time $t+1$, its angular frequency $\dot{\theta}$ increases and with it its phase angles 'margin' towards j increases. This leads to a higher angle difference θ_{ij} and hence to more power that can be transmitted, as $\sin(\theta_i(t+1) - \theta_j(t+1)) > \sin(\theta_i(t) - \theta_j(t))$.

Derivation of the Oscillator Equations

Next, we derive the nonlinear equations describing the development of the oscillators' states over time. For this we need to be able to calculate the change of the angular velocity of each oscillator. The derivation is based on the law of conservation of energy. It mostly follows from Filatrella et al. [FNP08], but tries to be more explanatory.

We have $N = |V|$ buses. For every bus $i \in V$ the total produced power $P_{\text{source},i}$ at a bus is equaled out by three other forms of power, given in Equation (4.4).

$$\underbrace{P_{\text{source,i}}}_{\text{generated power}} = \sum_{j=1, j\neq i}^{N} \underbrace{P_{\text{trans}_{ij}}}_{\text{transmitted power}} + \underbrace{P_{\text{acc},i}}_{\text{accumulated power}} + \underbrace{P_{\text{diss},i}}_{\text{dissipated power}} \tag{4.4}$$

The generated power $P_{\text{source,i}}$ is negative, if $i \in V$ represents a consumer. The power sent or received by bus i from another bus j is $P_{\text{trans}_{ij}}$. Accumulated power at bus i such as the kinetic power in a generator's flywheel is given by $P_{\text{acc},i}$. Finally, there is the thermal power loss $P_{\text{diss},i}$ which is the dissipated power at a bus i. The different power terms are defined as follows:

- Let $P_{\text{max}_{ij}}$ be the capacity of transmission line $\{i, j\}$:
$$P_{\text{trans}_{ij}} = -P_{\text{max}_{ij}} \sin(\theta_j - \theta_i) \qquad \forall \{i, j\} \in E$$
- Let $E_{\text{kin}} = I_i \cdot \frac{\dot{\theta}_i^2}{2}$ be the kinetic energy stored at bus i and I_i its moment of inertia. The moment of inertia determines the torque needed for the desired angular acceleration and is depending on what kind of machine we look at. Using the chain rule for ODEs this gives:
$$P_{\text{acc},i} = \frac{d}{dt} E_{\text{kin}} = \frac{1}{2} I_i \frac{d}{dt} (\dot{\theta}_i)^2 = I_i \dot{\theta}_i \ddot{\theta}_i \qquad \forall i \in V$$
- Let κ_i be the friction coefficient of the motor at bus i:
$$P_{\text{diss},i} = \kappa_i (\dot{\theta}_i)^2 \qquad \forall i \in V$$

Introducing these definitions to Equation (4.4) gives:

$$\begin{aligned} P_{\text{source},i} &= \kappa_i (\dot{\theta}_i)^2 + I_i \dot{\theta}_i \ddot{\theta}_i + \sum_{j=1, j\neq i}^{N} -P_{\text{max}_{ij}} \sin(\theta_j - \theta_i) \\ &\overset{4.2,4.3}{=} \kappa_i \Omega^2 + 2\kappa_i \Omega \dot{\phi}_i + \kappa_i \dot{\phi}_i^{\,2} + I_i \Omega \ddot{\phi}_i + I_i \dot{\phi}_i \ddot{\phi}_i + \left(\sum_{j=1, j\neq i}^{N} -P_{\text{max}_{ij}} \sin(\phi_j - \phi_i) \right) \end{aligned}$$

, where we used $\theta_i = \Omega t + \phi_i$ (4.2) and $\dot{\theta}_i = \Omega + \dot{\phi}_i$ (4.3). We want to solve the equations for the highest derivative:

$$I_i \Omega \ddot{\phi}_i = P_{\text{source},i} - \kappa_i \Omega^2 - 2\kappa_i \Omega \dot{\phi}_i - \kappa_i \dot{\phi}_i^{\,2} - I_i \dot{\phi}_i \ddot{\phi}_i + \left(\sum_{j=1, j\neq i}^{N} P_{\text{max}_{ij}} \sin(\phi_j - \phi_i) \right) \tag{4.5}$$

As we mentioned above, the phase changes are assumed to be small in comparison to the reference frequency $|\dot{\phi}_i| \ll \Omega$ for all $i \in V$. We therefore neglect all terms with $\dot{\phi}_i^{\,2}$ and $\dot{\phi}_i \ddot{\phi}_i$. Furthermore, to simplify the model it is usually assumed that the inertia and damping are the same for all machines and we simply use I and κ in all equations. This simplifies Equation (4.5) to:

$$I \Omega \ddot{\phi}_i = P_{\text{source},i} - \kappa \Omega^2 - 2\kappa \Omega \dot{\phi}_i + \left(\sum_{j=1, j\neq i}^{N} -P_{\text{max}_{ij}} \sin(\phi_j - \phi_i) \right) \tag{4.6}$$

In a last step we divide by $I\Omega$ and define abbreviations in Definition 4.1 in order to get the second order ODE.

Definition 4.1. *We set the system parameters to:*

$$P_i \coloneqq \frac{P_{source,i} - \kappa\Omega^2}{I\Omega} \tag{4.7}$$

$$\alpha \coloneqq \frac{2\kappa}{I} \tag{4.8}$$

$$K_{ij} \coloneqq \frac{P_{max_{ij}}}{I\Omega} \tag{4.9}$$

As above we have $P_i > 0$ for generators that produce electrical power and $P_i \leq 0$ for loads that consume it. In order for the system to synchronize and operate properly it is required that $\sum_{i=1}^{N} P_i = 0$, i.e., the amount of produced power equals the consumed.
The constant α, called the *effective damping factor*, accounts for the dissipated energy in a machine.
Parameter K_{ij} is called *coupling constant* for the transmission line between nodes i and j. If they are adjacent, its value is proportional to the line capacities, if not then it is zero. Following Witthaut et al. [WRZ+16b] it can also be retrieved from the grid parameters:

$$K_{ij} = \begin{cases} \frac{-B_{ij}\hat{U}_i\hat{U}_j}{I_i} & ,\text{if } \{i,j\} \in E \\ 0 & ,\text{if } \{i,j\} \notin E \end{cases}$$

, where $\hat{U}_i$ is the voltage magnitude at bus i and B_{ij} is the line susceptance of branch $\{i,j\}$. Furthermore, it is $K_{ij} = K_{ji}$ for all $i,j \in V$.

In the end this leaves us with an ODE system for the nonlinear behavior of N coupled oscillators representing a power grid. It is given by Equation (4.10).

$$\ddot{\phi}_i = P_i - \alpha\dot{\phi}_i + \sum_{j=1, j\neq i}^{N} K_{ij}\sin(\phi_j - \phi_i) \qquad i = 1,\dots,N \tag{4.10}$$

It consists of N ODEs of second order. System 4.10 is actually autonomous (2.16), since all time-dependent values ($\phi(t)$, $\dot{\phi}_i(t)$ and $\ddot{\phi}(t)$) are state variables and no external time-dependent value is present.

4.2. Synchronization

Formalizing and analyzing synchronization behavior in power grids is the purpose of the oscillator model. We want to be able to tell what happens after a perturbation took place. Perturbations can be of different nature: switching of transmission lines but also temporary load or demand peaks or even losses of generating units. If the disturbance is too heavy the utility frequency of the net is lost and it decomposes into desynchronized parts. According to Timme [Tim18], there are two types of synchrony that can be distinguished:

1. *Phase synchrony*: $\phi_i(t) = \phi_j(t) \quad \forall i,j \in V$
2. *Frequency synchrony*: $\dot{\phi}_i(t) = \dot{\phi}_j(t) \quad \forall i,j \in V$

The first case, also called identical synchrony, demands all oscillators to adopt the same phase and hence the same phase angle. For power grids such a state is undesirable, as the power flow on a transmission line $\{i,j\}$ is proportional to the sine of the phase difference of the two oscillators connected to it, see Equation (4.1). So in the case of $\phi_i = \phi_j$ we have $\sin(\phi_j - \phi_i) = 0$ and no power is transmitted.
Therefore, frequency synchrony is of more interest to us. The oscillators' phases differ but their frequencies (and hence their relative phase differences) are fixed and we get a constant amount of power transmitted between them.

Steady State

In the synchronized state the derivatives become zero: $\dot{\phi}_i(t) = \ddot{\phi}_i(t) = 0$ for all $i \in V$. This means all oscillators rotate at the reference frequency of 50 Hz and they do not change their rotational speed anymore. Equation (4.10) then becomes

$$0 = P_i + \sum_{j=1, j\neq i}^{N} K_{ij} \sin(\phi_j - \phi_i) \tag{4.11}$$

for all $i \in V$. Following Definition 2.18 this synchronized state is a fixed point of the oscillator equations. It is also called a *steady state*. These are the states we look at in the static model. It is only in the steady state that the phase differences $\phi_j - \phi_i$ are fixed pairwise and the power flow is well-defined, meaning it satisfies the KCL (Equation (2.4)) and KVL (Equation (2.5)). We know that the power transmitted on the grid's transmission lines $\{i, j\} \in E$ is proportional to the sine of the relative phases of two connected oscillators. Hence, the power flow between bus i and j can be defined as in Equation (4.12) [Tim18].

$$F_{ij} = K_{ij} \sin(\theta_j - \theta_i) \tag{4.12}$$

By considering the coupling value as line capacity K_{ij} we define the *relative load* L_{ij} of a transmission line in Equation (4.13) [Tim18]. It is $L_{ij} \in [0, 1]$ which gives the fraction of how much the line is utilized.

$$L_{ij} = \frac{F_{ij}}{K_{ij}} = \sin(\theta_j - \theta_i) \tag{4.13}$$

Mean-Field

A way to measure the level of the system's synchrony comes from mean-field theory. By averaging over the phases of the N oscillators we can get some useful insights into the synchronization behavior. We assume that the oscillators are located around the unit circle in the complex plane. The *synchronization order parameter* states whether they rotate synchronously around that circle or if they rather act on their own. It is given by Equation (4.14) [Tim18], where we calculate the geometric center of all the phases by summing up their momentary phases in complex exponential form $\phi_j(t) = e^{i\phi_j}$ and normalizing by the number of oscillators N.

$$re^{i\psi} = \frac{1}{N} \sum_{j=1}^{N} e^{i\phi_j} \tag{4.14}$$

The resulting complex number is the geometric center. Its argument $\psi \in [0, 2\pi)$ is the *average phase* and the absolute value $r \in [0, 1]$ is the *phase coherence*. In physics, two waves are coherent if their phase difference is constant. This also means that they have the same frequency, as the phase difference can only remain the same if the waves develop with the exact same speed.

For oscillators the intuition behind this equation now is the following: Imagine them as a swarm of points rotating on the complex unit circle with their position defined by their current phase as depicted in Figure 4.2. The closer they are clumped together the closer to the unit circle the geometric center will be. The coherence will become $r = 1$, if all points are in the same spot. This corresponds to phase synchrony which is, as mentioned in Section 4.2, undesirable. If r is very small the points are evenly scattered around the circle. This corresponds to an unsynchronized network. So what is ideal? As we saw in Section 3.1 **A3** the phase angle differences in a power grid usually are quite small with a few degrees. So a value close to but not exactly one is what indicates good operation.

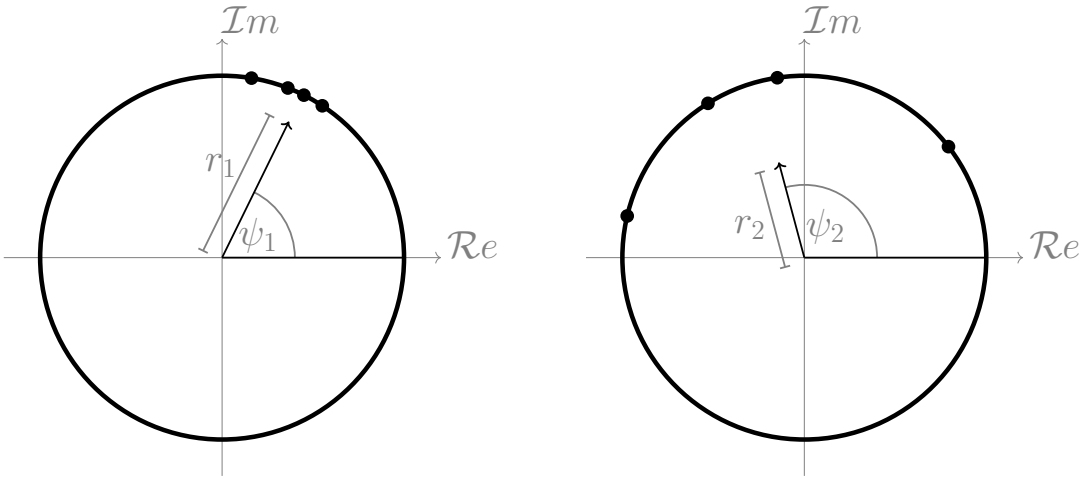

Figure 4.2.: Illustration of phase coherences. The oscillators on the left are grouped together more tightly than on the right. Consequently, the phase coherence is larger $r_1 > r_2$. Angles ψ_1 and ψ_2 are the average phases.

5. Transient Network Analysis

In this chapter we present the methods used for analyzing the quality of switchings based on DTP-betweenness in terms of system stability and synchronization. Since the linear DC model of Chapter 3 does not consider any dynamic behavior the question is how good these switchings are in the real world. We perform a quantitative analysis on sample power grids in order to establish whether the removed edges would keep our network in an operable state or if net synchronization will be lost.

In order to do so, we use the oscillator model of Chapter 4 to formulate the ODEs describing the power grid's dynamics. Then we calculate the DTP-betweenness 3.9 and successively switch out each edge depending on its betweenness value. Next, we apply two methods for analyzing the resulting network. The first one is a *small-signal analysis* and is based on Lyapunov's first method [KBL94]. that assesses system stability at a certain point in time via linearization. The second one is a numerical integration to simulate the development of a systems behavior over time.

5.1. Setup

We setup the model by making some assumptions and rephrasing the oscillator equations. There are three phases we can distinguish during the analysis. The *pre-switching* phase during initialization and 'normal operation'. The *on-switching* period, during which the switching takes place. And the *post-switching* phase, in which the effects of the switching manifest. In this work we assume the switching duration to be zero, i.e., happens instantaneous. We therefore only consider pre- and post-switching states.
Additionally, we switch only one edge at a time, in order to be able to directly compare the betweenness with the stability and post-switching behavior.

When we want to evaluate a test power grid we read its *case file*. It contains information about the network topology and the electrical branch and bus properties. The case file represents the power grid in a pre-switching steady state, where power generation and demands are equaled out.

Let us take the system equation 4.10, to describe the dynamics of a power grid we want to study. Before we can proceed, this second order system needs to be reduced to first order ,i.e., a set of ODEs with only first derivatives. To achieve this we introduce a new variable $\omega_i = \dot{\phi}_i$ as a substitute for the first derivative of ϕ_i. The system then reads as follows:

$$\dot{\phi}_i = \omega_i \qquad i = 1, 2, \ldots, N \tag{5.1}$$

$$\dot{\omega}_i = \underbrace{P_i - \alpha\omega_i + \sum_{j=1, j\neq i}^{N} K_{ij} \sin(\phi_j - \phi_i)}_{=f_i(\boldsymbol{\phi}, \boldsymbol{\omega})} \qquad i = 1, 2, \ldots, N \tag{5.2}$$

where N is the number of buses. This leaves us with $2N$ equations of first order. In vector notation this is:

$$\begin{pmatrix} \dot{\phi}_1 \\ \vdots \\ \dot{\phi}_n \\ \dot{\omega}_1 \\ \vdots \\ \dot{\omega}_n \end{pmatrix} = \begin{pmatrix} \omega_1 \\ \vdots \\ \omega_n \\ f_1(\boldsymbol{\phi}, \boldsymbol{\omega}) \\ \vdots \\ f_n(\boldsymbol{\phi}, \boldsymbol{\omega}) \end{pmatrix} \tag{5.3}$$

a state of the first order system is then given by $(\phi_1, \ldots, \phi_n, \omega_1, \ldots, \omega_n)$.

When we want to switch an edge $\{i, j\}$ between two nodes i and j we set the coupling between them to $K_{ij} = 0$.

5.2. Small-Signal Analysis

Small-signal analysis is used in electronics engineering to approximate the behavior of nonlinear AC circuits. This method can also be used on the nonlinear oscillator model of the power grid we are looking at. The idea is that we do not compute the development of the system over the whole time. We rather want to assess whether our dynamical system is in a stable state after switching took place. For this we try to find an equilibrium point for the altered system. We then look at the linearization of the system equations at this point which gives us the Jacobian matrix. The idea of small-signal analysis is that when we look at the system in a close area around an equilibrium point it behaves pretty much like the linearized version of it. The reason we now can deduce a prediction on the behavior of the system comes from Lyapunov's first method for stability [KBL94, p. 706]. When evaluate the eigenvalues of the Jacobian they tell us if the system next to our evaluation point is going to be stable or unstable.

Following the procedure presented in [KCG+19] the small-signal analysis can now be performed by the following steps:

Step 1 Initialization. Read in the case file of the power grid. Then compute the power flow for the pre-switching steady state of the network to retrieve the initial network values before the switching takes place. These values include the generator or load power P_i, as well as the phase angles ϕ_i at the different buses. We calculate the DC power flow from Equation (3.1), as this is the usual procedure for the oscillator model. Systems with a well-defined power flow are in an equilibrium state of which we know that the time derivatives, i.e., the angular frequency $\dot{\phi}$ and the acceleration $\dot{\omega}$ are zero. Equations (5.1) and (5.2) become Equations (5.4) and (5.5) respectively.

$$0 = \omega_i \qquad i = 1, 2, \ldots, N \tag{5.4}$$

$$0 = P_i + \sum_{j=1, j\neq i}^{N} K_{ij} \sin(\phi_j - \phi_i) \tag{5.5}$$

Step 2 As mentioned above, we assume that the switchings takes place instantaneously. We determine the post-switching equilibrium point (see Definition 2.18) $\boldsymbol{a} \in \mathbb{R}^{2N}$ with

$$\boldsymbol{a} = (\phi_1^e, \ldots, \phi_N^e, \omega_1^e, \ldots, \omega_N^e)$$

by solving the system of nonlinear equations 5.5 to get $f_i(\boldsymbol{a}) = \mathbf{0}$ for all $i = 1, 2, \ldots, N$ (Equation (5.4) is satisfied trivially). This can be done for example using the Newton-Raphson algorithm or Powell's hybrid method [PTVF07]. The algorithm is initialized with the phase angles ϕ_i from step 1.

Step 3 Linearize the system of Equations (5.1) and (5.2) for the determined values of the equilibrium point $\boldsymbol{a}$. This is done using the linearization principle which takes the first two terms of the Taylor's series expansion of the system equations.

$$\begin{pmatrix} \dot{\phi} \\ \dot{\omega} \end{pmatrix} = \begin{pmatrix} \omega^e \\ f(\boldsymbol{a}) \end{pmatrix} + \boldsymbol{J}(\boldsymbol{a}) \cdot (\begin{pmatrix} \phi \\ \omega \end{pmatrix} - \boldsymbol{a}),$$

where $\omega^e = (\omega_1^e, \ldots, \omega_N^e)$ and $\boldsymbol{J}(\boldsymbol{a}) \in \mathbb{R}^{2N \times 2N}$ is the Jacobian matrix of the system at point $\boldsymbol{a}$. This approximates the behavior of the system in a close area around $\boldsymbol{a}$ reasonably accurate. Abbreviating $f_i(\boldsymbol{\phi}, \boldsymbol{\omega})$ with f_i, the Jacobian reads as follows:

$$\boldsymbol{J} = \begin{pmatrix} \frac{\partial \dot{\phi}_1}{\partial \phi_1} & \cdots & \frac{\partial \dot{\phi}_1}{\partial \phi_n} & \frac{\partial \dot{\phi}_1}{\partial \omega_1} & \cdots & \frac{\partial \dot{\phi}_1}{\partial \omega_n} \\ \vdots & \ddots & \vdots & \vdots & \ddots & \vdots \\ \frac{\partial \dot{\phi}_1}{\partial \phi_n} & \cdots & \frac{\partial \dot{\phi}_n}{\partial \phi_n} & \frac{\partial \dot{\phi}_n}{\partial \omega_1} & \cdots & \frac{\partial \dot{\phi}_n}{\partial \omega_n} \\ \frac{\partial f_1}{\partial \phi_1} & \cdots & \frac{\partial f_1}{\partial \phi_n} & \frac{\partial f_1}{\partial \omega_1} & \cdots & \frac{\partial f_1}{\partial \omega_n} \\ \vdots & \ddots & \vdots & \vdots & \ddots & \vdots \\ \frac{\partial f_n}{\partial \phi_1} & \cdots & \frac{\partial f_n}{\partial \phi_n} & \frac{\partial f_n}{\partial \omega_1} & \cdots & \frac{\partial f_n}{\partial \omega_n} \end{pmatrix} \tag{5.6}$$

Evaluating these terms leaves us with the following matrix:

$$\boldsymbol{J} = \begin{pmatrix} \mathbf{0} & \boldsymbol{I} \\ \boldsymbol{F} & \alpha \cdot \boldsymbol{I} \end{pmatrix} \tag{5.7}$$

, where $\mathbf{0} \in \mathbb{R}^{N \times N}$ is the zero matrix, $\boldsymbol{I} \in \mathbb{R}^{N \times N}$ is the identity matrix and $\boldsymbol{F} \in \mathbb{R}^{N \times N}$ reads:

$$\boldsymbol{F}_{(i,j)} = \frac{\partial f_i}{\partial \phi_j} = \begin{cases} (-1) \cdot \sum_{k=1, k \neq i}^{N} K_{ik} \cos(\phi_k - \phi_i) & , i = j \\ K_{ij} \cos(\phi_j - \phi_i) & , i \neq j \end{cases} \tag{5.8}$$

with $i, j = 1, 2, \ldots, N$.

Step 4 Now we test the equilibrium point for stability [LK07]. In order to do so we calculate the eigenvalues of $\boldsymbol{J}$. There are $2N$ linearly independent eigenvectors and hence $2N$ eigenvalues λ_i, corresponding to the Jacobian's dimensions. If all eigenvalues have negative real parts we can deduce that the equilibrium point is stable. If one or more of the eigenvalues has a positive real part the system is in an unstable state. In the case that one or more eigenvalues have a real part of zero and the rest have negative real parts we cannot make any conclusions for certain and the system requires further investigation such as numerical integration [KPA+04, p. 706]. Summarizing:

1. $\mathrm{Re}(\lambda_i) < 0 \ \forall i = 1, 2, \ldots, 2N \Rightarrow$ the equilibrium point is stable
2. $\exists i \in \{1, 2, \ldots, N\} : \mathrm{Re}(\lambda_i) > 0 \Rightarrow$ the equilibrium point is not stable
3. $\mathrm{Re}(\lambda_i) \leq 0 \ \forall i = 1, 2, \ldots, 2N \wedge \exists i : \mathrm{Re}(\lambda_i) = 0 \Rightarrow$ further investigation necessary

Since the eigenvalue computation of large matrices is based on numerical algorithms we round off to zero if values are sufficiently small enough, i.e., $\mathrm{Re}(\lambda_i) < 1 \times 10^{-13}$. Finally, the computations on this matrix will always yield one eigenvalue $\lambda = (0, 0)$. According to [SRM+18] this eigenvalue corresponds to the global shift of the oscillators phase angles. It therefore can be omitted as it has no physical relevance and does not give information on the system stability.

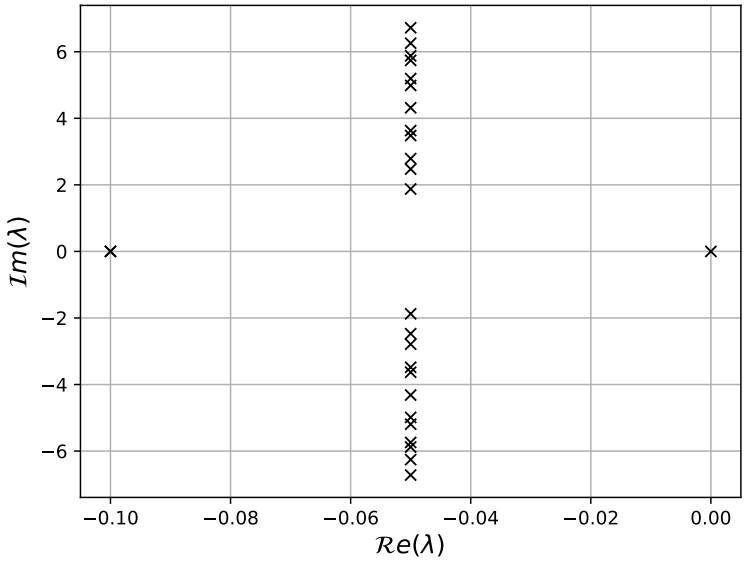

Figure 5.1.: Eigenvalues for `nesta_case14_ieee_rts` after switching edge $e_{13} = \{6, 7\}$. The x- and y-axis correspond to the real and imaginary axis respectively.

Figure 5.1 shows the computed eigenvalues for $\boldsymbol{J}$ after switching edge e_{13} in the graph corresponding to case file `nesta_case14_ieee_rts`. We can see their values on the imaginary and real axis. In this case there is an eigenvalue $(0, 0)$ and therefore we cannot say for sure whether the system is going to be stable or not. The symmetry comes from the following fact:

Corollary 5.1. *Let $\boldsymbol{v} \in \mathbb{C}^N$ be an eigenvector of $\boldsymbol{J}$ with eigenvalue $\lambda \in \mathbb{C}$. Let $\overline{\boldsymbol{v}}$ be the complex conjugate of $\boldsymbol{v}$. Then $\overline{\boldsymbol{v}}$ is an eigenvector of $\boldsymbol{J}$ as well with eigenvalue $\overline{\lambda}$.*

Surprisingly, for a lot of system configurations the majority of the resulting eigenvalues have a real part of -0.05 and there is one eigenvalue $\lambda = (-0.1, 0)$. Unfortunately, we were not yet able to investigate this observation. The values can certainly be linked to properties of the Jacobian and the symmetries in its submatrices and may provide further insight into the properties of the system equations.

5.3. Simulation

Beyond the stability analysis we also perform simulations in order to visualize the synchronization behavior of the power grid in regular and critical cases and to give some

comparison to the eigenvalue computations. We also compute the mean-field mentioned in Section 4.2. The oscillator system equations of first order 5.1 and 5.2 are solved numerically over a given time frame by approximating their integral. Numerical integration solves ODEs iteratively over discrete, yet sufficiently small, time steps. One of the best known algorithms for this is the *classic Runge-Kutta method* [PTVF07], the fourth-order version of this family of integration methods.

As in Section 5.2 we set up the system with a DC-power flow calculation to retrieve the initial phase angles ϕ_i for the oscillators. The initial frequencies ω_i are set to zero, as they describe the deviation from the utility frequency of 50Hz and we assume a stable operating grid in the beginning.
We now give a first illustration of how the simulations work based on the `nesta_case3_pjm` case file of the NESTA data set[CGS14]. Figure 5.2 shows the underlying graph before and after switching edge $e_1 = \{1, 2\}$. The arrows are there to imply the direction of the power flow.

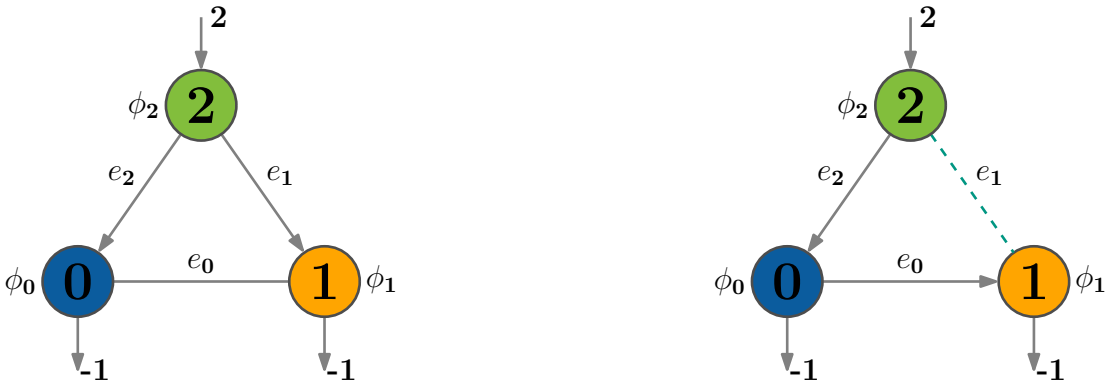

(a) Graph before switching.

(b) Graph after switching edge e_1.

Figure 5.2.: Underlying graph of `nesta_case3_pjm` power grid before and after switching of edge $e_1 = \{1, 2\}$. The gray arrows imply the load flow direction. Node 2 is the generator and node 0 and 1 are loads. The ϕ_i are the phase angles at nodes i respectively.

Figure 5.3 shows how the phases of the three oscillators corresponding to the nodes develop over time. Oscillator 1 is a generator, with a power term of $P_1 = 2.0$, i.e., producing 2 units of power. Oscillators 0 and 1 are loads with $P_0 = P_2 = -1.0$. We can see their phases oscillate heavily in the beginning while they converge towards a synchronized state. The phases of the loads approach the same value while the generator's phase is higher. As we saw in Section 4.1, $\phi_1 > \phi_0$ and $\phi_1 > \phi_2$ implies power is flowing from node 1 to nodes 0 and 2 which is exactly what we would expect.
Now, we observe the system after it started to settle down beginning from time step 80. The switching takes place at $t_0 = 100$ and edge e_1 is removed. This causes the load flow to redirect and alters the phases accordingly. Phase ϕ_1 increases as all power now has to be routed through node 0 and ϕ_2 drops as it receives its power through node 0 whose phase stayed the same. With this the system converges to a new state with the phase differences corresponding to the new load flow.

Figure 5.4 shows how the frequencies develop for the same network and switching operation of Figure 5.3. We can see that oscillating phases correspond to oscillating frequencies. When they begin to settle, we see that the nodes eventually synchronize their frequencies at 0 which means that their oscillations are $\dot{\theta} = \Omega + 0 = 2\pi \cdot 50$ Hz, i.e., at the desired utility frequency. In the limit this network state corresponds to a frequency synchronized grid as defined in Section 4.2 with $\dot{\phi_0} = \dot{\phi_1} = \dot{\phi_2}$.

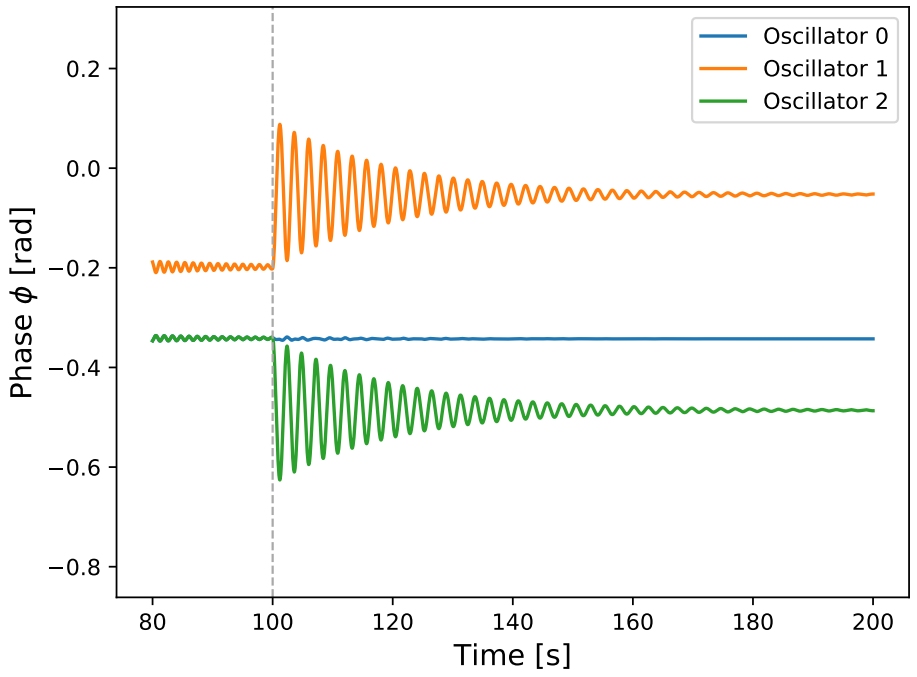

Figure 5.3.: Phase development for `nesta_case3_pjm`. The y-axis shows phase angles ϕ_i of the three oscillators wrt. the reference frame $\theta_i(t) = \Omega t + \phi_i(t)$. The x-axis shows the time t. Producer: Oscillator 1 (■) with $P_1 = 2.0$. Loads: Oscillators 0 (■) and 2 (■) with $P_0 = P_2 = -1.0$. At $t_0 = 100$ edge {1,2} is switched out.

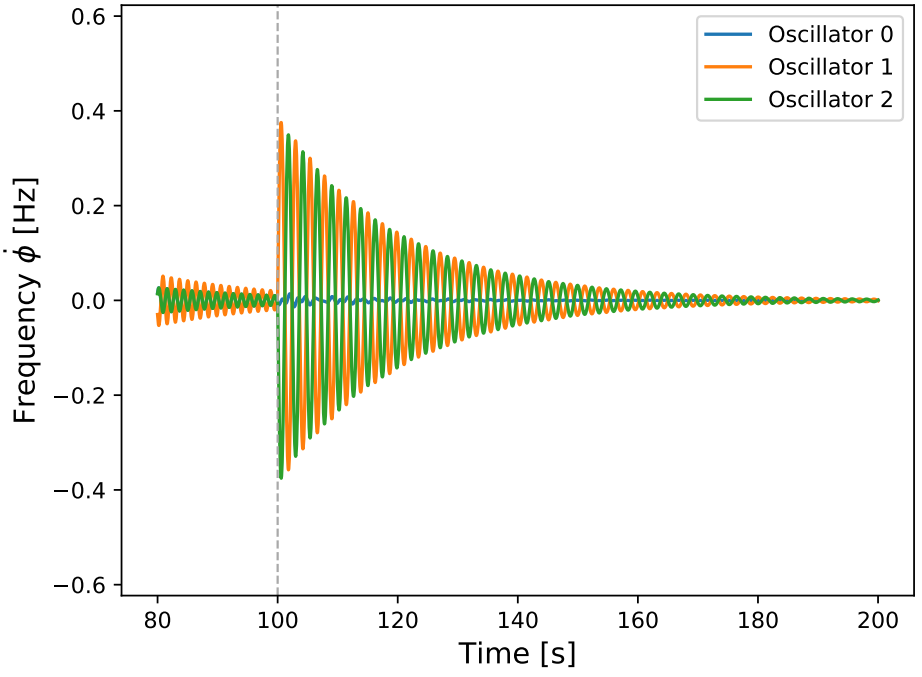

Figure 5.4.: Frequency development for `nesta_case3_pjm`. The y-axis shows the frequency deviation $\dot{\phi}_i(t)$ from the reference frame in Hz. The x-Axis shows the time t. At $t = 100$ edge {1,2} is switched out.

6. Evaluation

In this chapter we present our results based on the models developed in Chapters 3 and 4 using the methods of Chapter 5. We start with some information on the used software and data for the evaluation process followed by some important chosen parameters. Next, we present the hypotheses with our findings and finally we have some closing remarks where we discuss general observations some considerations concerning the modeling.

6.1. Implementation

The dataset we performed our analysis on is the NICTA Energy System Test Case Archive (NESTA) [CGS14]. This dataset provides a comprehensive collection of refined power system test case files with more realistic data such as better thermal line limits or phase angles. It brings together case files that were developed over the past decades from several different research platforms such as MATOPWER [ZMsT+11] or IEEE [UoW14]. The files represent a power grid in a steady state and are usually used for power flow studies.

The analysis procedure was implemented in C++ using several numerical computation libraries. Furthermore, we made use of the Energy Grid Optimization and Analysis (EGOA)[1]-tool which is designed for graph-based power grid analysis, planning and optimization algorithms. The tool provides case file parsing since all NESTA data is stored in a matlab format. It also contains power flow calculation, graph-theoretic algorithms and more. We calculated the initial power flow in step 1 with a DC-power flow method using the tool. The DTP-edge betweenness was also computed using EGOA. In the small-signal analysis implementation we used the GNU scientific library (GSL) [G+18], a numerical library, for nonlinear equation solving when determining the post-switching SEP. We also made use of the Eigen linear algebra library [GJ+10] for eigenvalue computation. The numerical integration of the oscillator model was performed using the Boost library [Sch14], more precisely the ODEINT-package [AM11] which is designed for solving initial value problems of ordinary differential equations.

6.1.1. Model Parameters

Next we show the relevant model and simulation parameters. Table 6.1 shows the used default values that were used if not mentioned otherwise in this chapter. The first three values are the parameters from Equation (4.10) and are taken from literature, see e.g. the

[1] https://github.com/franziska-wegner/egoa

Parameter	Default Value	Description
α	0.1	Effective damping factor
K	7.0	Global coupling constant
P_i	$\pm$ 1.0	Power term of generator/load
T	200	Total time frame
Δt	0.05	Integration time steps
t_0	100	Time point of switching event

Table 6.1.: Simulation parameters and their default values.

works of Rhoden et al.[RJTK16] or Schäfer et al. [SWTL18]. A common assumption there is to set the coupling values equal for all edges. This means there is a global coupling constant K and we set $K_{i,j} = K$, if $\{i, j\} \in E$ and $K_{ij} = 0$ otherwise. We point out that these values are generalizations and simplifications that may not always resemble the actual power grid perfectly. For further discussion on this see Section 6.3.
The time parameters were estimated on our own. The time range per event is 100 s which leads us to a total simulation time of $T = 200$ for the pre-switching and the post-switching phase combined. With the transient behavior usually happening instantaneously and then decaying during the next 30 to 50 seconds rather quickly for synchronization this proves to be a suitably large time frame. The chosen integration step size is $\Delta t = 0.05$ which is a compromise between a high enough sampling rate and computational efficiency. The switching event takes place at time $t_0 = 100$. For the ideal choice of time range and step size further investigations will be required.

6.2. Results

We now present the hypotheses we studied during this work. The structure is as follows. We first give some background information and considerations on the suspected behavior to happen in the power grid. We then formulate a hypothesis regarding this and finally present our experimental results and discuss them.

Quality of the Switching Heuristic

The intuition behind a Dominating Theta Path (DTP) 3.8 is that it limits the transmitted power between a source and a target node in a graph due to its susceptance or thermal capacity values. The more often an edge is situated on a DTP the more limiting paths can be resolved by removing this edge. Our first question now was whether the suggested switching based on the highest DTP-betweenness centrality-value c_{DTPB} 3.9 keeps our power grid in an operable state or if it desynchronizes. Our assumption was that switching in fact leaves the grid in tact. We base this on the intuition that DTPB can be understood as a metric for how much at risk a transmission line is to become congested. This would mean, removing the line that can easiest reach its operational limits should be beneficial for grid stability. In addition to this we assume that the removal of an edge with a higher c_{DTPB}-value also increases the chance that the remaining network continues stable operation.

Hypothesis 1. Switchings based on DTPs using a DC-approximation yield a stable operating power grid. Moreover, switching an edge with a higher c_{DTPB}-value is more likely to maintain the network's stability.

Our approach was as follows. We first calculated the DTP-betweenness for all edges. Next we sorted the edge IDs descending according to their betweenness values. We then iteratively switched edge by edge and quantified the resulting system stability. We performed the small-signal analysis of Section 5.2 as well as numerical integration from Section 5.3.

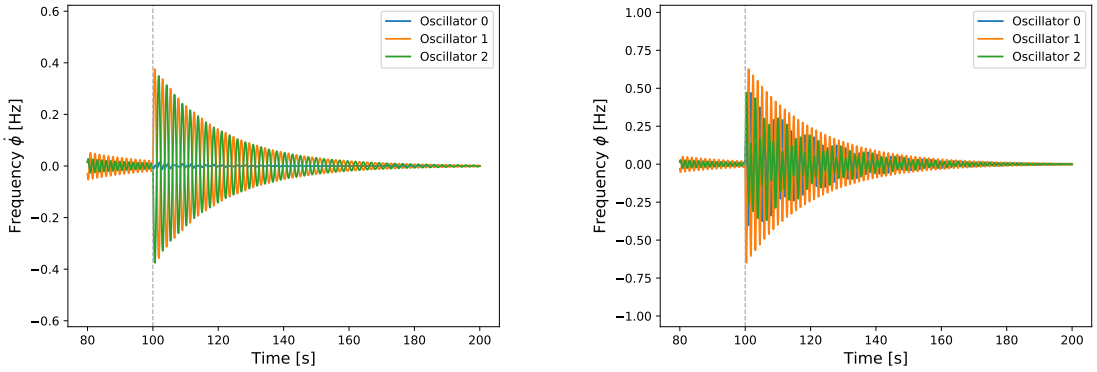

(a) Switching of edge e_1 with $c_{\mathrm{DTPB}} = 1.0$.

(b) Switching of edge e_0 with $c_{\mathrm{DTPB}} \approx 0.33$.

Figure 6.1.: Comparison of frequency synchronization after switching for two edges with different c_{DTPB}-values for the `nesta_case3_pjm` case file. The y-axis shows the frequency deviation from the reference frame of 50 Hz. The switching takes place at $t = 100$.

Figure 6.1 gives a first hint that a higher c_{DTPB}-value in fact can correlate to less disturbance of the net frequency. We compare the resulting oscillators' frequencies after switching a single edge in the `nesta_case3_pjm` network that we already saw in Section 5.3. Removing edge $e_1 = \{1, 2\}$ in Figure 6.1a with $c_{\mathrm{DTPB}}(e_1) = 1$ - the highest value for this case - gives a maximal frequency amplitude of $\phi_i \approx 0.4$. This is a significantly smaller reaction compared to the switching of $e_0 = \{0, 1\}$ with $c_{\mathrm{DTPB}}(e_1) \approx 0.33$ which results in a peak of $\phi_0 \approx 0.6$ in Figure 6.1b.

The overall results for all edges of a power grid can be seen in Figure 6.2. In this example we applied the analysis to the `neasta_case39_epri` whose topology is shown in Figure 6.3. The plot shows the stability for the system after switching a certain edge. As before, the edges are sorted by their c_{DTPB}-value in descending order, indicated by the green line. The blue marks show what the small-signal analysis revealed when we computed the eigenvalues of the system's Jacobian. If there exists an eigenvalue with real part 0 we call the system state *critical*. As we can see, eleven switchings left the system in a critical state for which we cannot guarantee a stable operation afterwards. Interestingly there exists a group of edge switchings resulting in a critical state that all had the same c_{DTPB}-value, as the plateau in the plot shows. These edges are marked orange in Figure 6.3. As we can see these are edges connecting leaf nodes or lie on a path to a leaf. Removing these edges disconnects the power grid and hence has a more severe effect on system stability.
With the current parameter configuration we do not observe any unstable switchings. This changes rapidly when reducing the coupling value K. We discuss in Section 6.3 the reason for the choice of our coupling and acknowledge that it requires further studies incorporating more finely tuned coupling parameters for a more realistic representation of the real world.

What we saw overall was that the removal of the edges with highest c_{DTPB}-value in fact resulted in a stable state according to the stability values of the eigenvalue analysis. This was also verified in most cases by numerical integration. On the other side however, we could not make any direct link between critical or unstable states and the edges with the

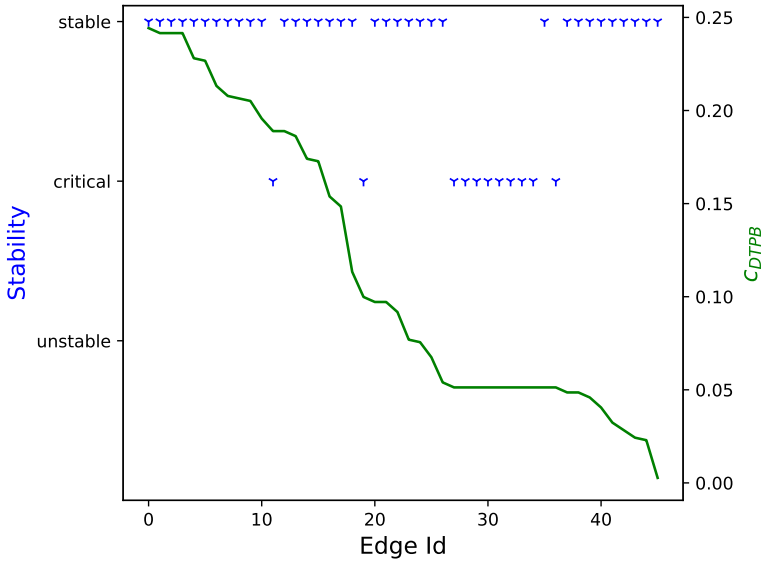

Figure 6.2.: Stability compared to the DTP-betweenness of an edge for the `nesta_case39_epri` case file. The x-axis shows which edge is switched out where the edges are ranked in decreasing order by their c_{DTPB}-values. The left y-axis shows the three possible stability states of the small-signal analysis (blue dots). The y-axis on the right side shows the c_{DTPB}-values (green line).

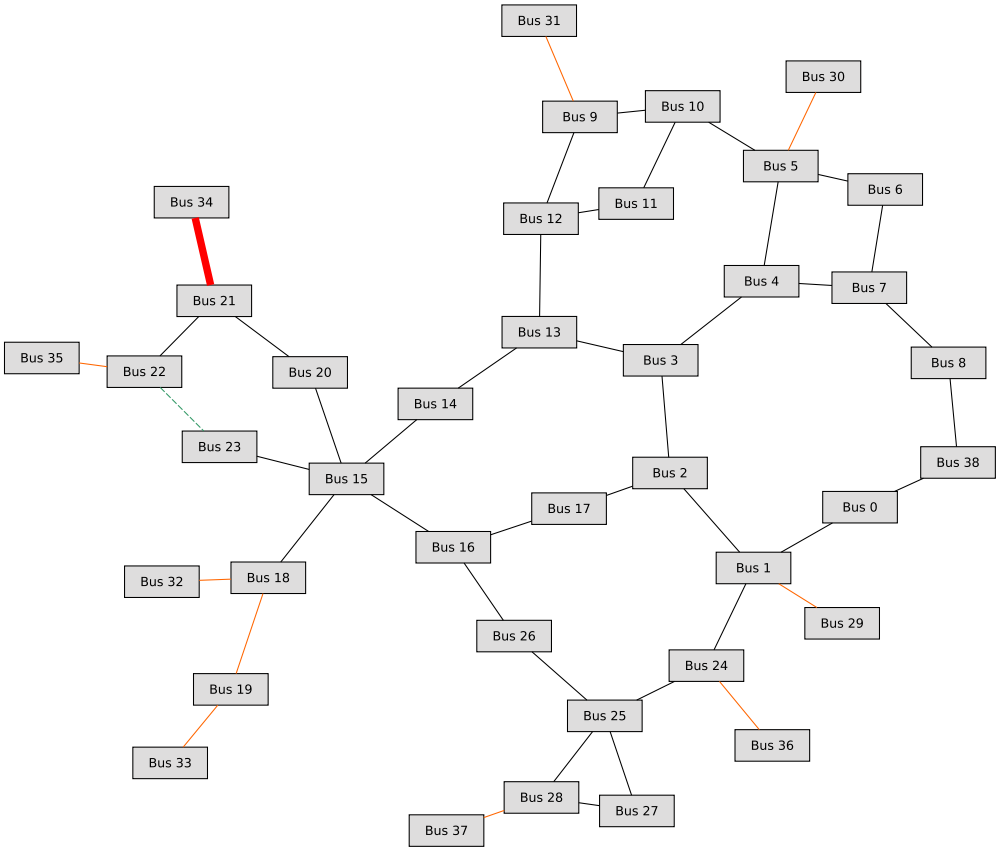

Figure 6.3.: A graph representation for the `nesta_case39_epri` network. The highlighted edges (■) are critical edges. They are all bridges connecting end nodes. The image shows also that after the edge between bus 22 and 23 is removed (dashed line), the edge between bus 21 and bus 34 gets congested (■).

lowest c_{DTPB}-value. We can see that in a lot of cases the system is considered to be in a stable state. Yet, even though the oscillators synchronize eventually the reaction to the switchings vary, as we saw in Figure 6.1, and may be harmful as well if the frequency amplitudes exceed a certain threshold.

Additional results on other test cases can be found in the appendix in Section A.

Load Redistribution

Witthaut et al. [WRZ+16a] show that after a transmission line is removed we have to take into account the load redistribution on alternative paths over which the power is going to be rerouted. The question is, how big the impact of the redistribution is going to be. Our assumption is to see a correspondence between the load flow redistribution and the c_{DTPB}-value of the removed edge.

Hypothesis 2. Switching an edge with higher c_{DTPB}-value causes less load redistribution in the network.

The load of an edge in the oscillator model was defined in Equation (4.13) as $L_{ij}(t) = \sin(\phi_j(t) - \phi_i(t))$. Let $L_{ij}^1 = L_{ij}(t_0 - \Delta t)$ be the load on the edges right before a switching takes place. Let $L_{ij}^2 = L_{ij}(T)$ be the edge load at the end of the simulation, after the switching took place and the system had time to settle down.
Figure 6.4 shows the results for switching edge $e_6 = \{2, 17\}$ with the highest and edge $e_{37} = \{22, 23\}$ with the lowest c_{DTPB}-value in the `nesta_case39_epri` network. The black marks indicate how heavily an edge was loaded before switching (L_{ij}^1) and the red ones how much it was afterwards (L_{ij}^2). A value of 1.0 means the edge has reached its capacity limit. We can see that the load redistribution for switching e_6 in Figure 6.4a is significantly less severe than for e_{37} in 6.4b. Another observation is that the heavily loaded edges in 6.4b correspond to the ones whose switchings were classified as critical in Figure 6.2. The edges with heavier load changes are the bridges marked in Figure 6.3. Edge e_{37} is the dashed line. With its switching the cycle it was on is interrupted and edge $\{21, 34\}$ becomes congested with a load very close to one. The correspondence between overloading and instable switchings can also be observed for other case files.

However, we have to keep in mind that the edges have varying loads and that the results are influenced by how heavily a removed edge was loaded. So we want to see whether we get an overall correspondence between c_{DTPB}-values and the absolute load redistribution that is taking place over all switchings. Our assumption here is that more load distribution causes more stress to the network and is potentially more dangerous.
We calculate the absolute switching load difference on edge $e = \{i, j\}$ by $|L_{ij}^1 - L_{ij}^2|$ for all edges $e \in E$. The *accumulated load difference* is denoted by $\Delta L_{ij_{acc}}$ and is given by:

$$\Delta L_{ij_{acc}} \coloneqq \sum_{\{i,j\} \in E} |L_{ij}^1 - L_{ij}^2| \tag{6.1}$$

Figure 6.5 shows the accumulated load difference for two datasets. The expected inverse proportional behavior of load redistribution to DTP-betweenness can be seen in Figure 6.5a and was also observed for other case files. There are however some cases for which the expected behavior could not be shown as we see in Figure 6.5b. The $\Delta L_{ij_{acc}}$-values for the switchings with highest c_{DTPB}-values are still relatively low, yet, the peak in load redistribution is certainly not where we would have expected it to be.

Among the studied case files the `nesta_case189_edin` network takes a special role. It represents the Iceland power grid and has a more hierarchical structure than the others.

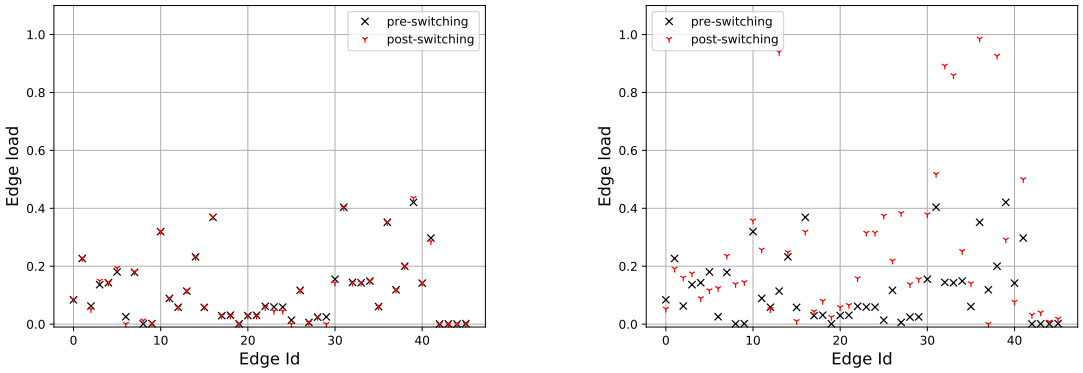

(a) Load redistribution after Switching of edge e_6 with $c_{\mathrm{DTPB}} \approx 0.244$.

(b) Load redistribution after Switching of edge e_{37} with $c_{\mathrm{DTPB}} \approx 0.003$.

Figure 6.4.: Comparison of the edge loads L_{ij}^1 before (■) and L_{ij}^2 after switching (■) for the edge with the highest c_{DTPB}-value (e_6) and the one with the lowest (e_{37}). for the `nesta_case39_epri` case file. The y-axis shows the utilization of every edge. Black marks are before switching, red marks afterwards. The x-axis shows all edges in the network.

This means there are more tree-like subgraphs present and hence a lot more bridges that disconnect several buses from the rest of the network at once when switched out. The consequence is the loss of several generators and/or loads that the remaining sub-networks have to compensate for. Often the edges with c_{DTPB}-values between 0.08 and 0.17 are such bridges. These are the edges that show the most load redistribution in Figure 6.5b.

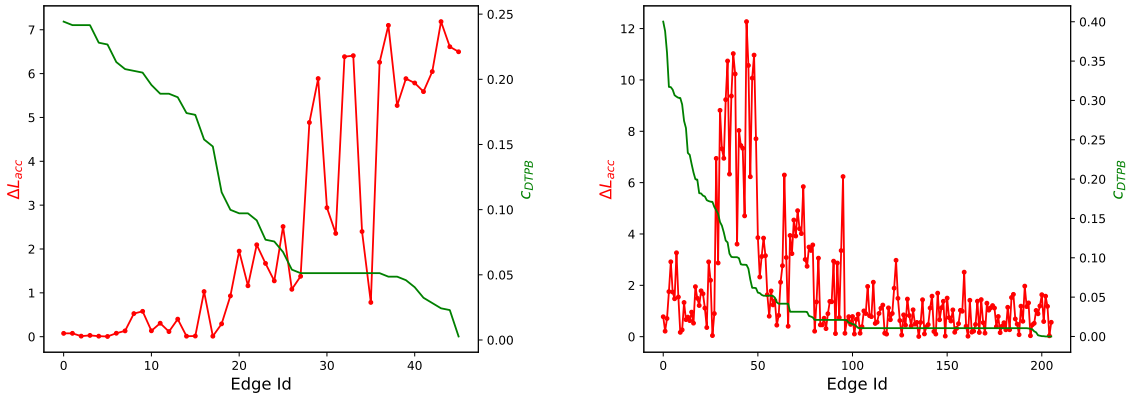

(a) `nesta_case39_epri`

(b) `nesta_case189_edin`

Figure 6.5.: Accumulated load difference in comparison to c_{DTPB}-values for two case files. The x-axis shows the switched edges in decreasing order by their c_{DTPB}-values. The left y-axis shows represents the $\Delta L_{ij_{acc}}$-values (red line). The y-axis on the right side shows the c_{DTPB}-values (green line).

Additional results on other test cases can be found in the appendix in Section A.

Betweenness and Mean-Fields

In Equation (4.14) we defined the mean-field equation that gives the phase-coherence of the oscillators at time t. When we now run a simulation for an extended period of time

and compute the average coherence $r_{mean} \in [0, 1]$ we can tell how the system evolves over time. It is defined as follows [Tim18]:

$$r_{mean} := Re\left(\frac{1}{N}\langle|\sum_{i=1}^{N} e^{i\phi_j(t)}|\rangle_t\right) \tag{6.2}$$

, where $\langle|\cdot|\rangle_t$ gives the average value of all time points $t = (t_0, t_0 + \Delta t, \ldots, T)$ as we are interested in the post-switching state after time t_0.

Since the average phase coherence value is used to to give an overview of the synchronization behavior over time, we also would like to link it to the betweenness values as we did before. The assumption again is that switching an edge with higher c_{DTPB}-value gives a higher r_{mean} value compared to edges with smaller values.

Hypothesis 3. r_{mean} is correlated to c_{DTPB}.

Figure 6.6 shows our findings for the already discussed case files. As we can see again, the results differ. In Figure 6.6a the mean-field values mostly correspond to the betweenness values. Figure 6.6b on the other hand represents a situation where this correspondence was not achieved. Again, as for Hypothesis 2, the hierarchical structure and thereby presence of numerous bridges in the `nesta_case189_edin` leads to a decomposition of the network when switching. The consequence to the loss of several buses at once is the loss of synchronization. In general however most of our results showed rather high r_{mean}-values that diminished with switchings of lower c_{DTPB}-valued edges.
Note, while r_{mean}-values of around 0.6 do not necessarily mean the network is desynchronized, it is usually the case. Only values above 0.8 or 0.9 are the ones representing rather strong frequency synchronization, see Section 4.2.

Additional results on other test cases can be found in the appendix in Section A.

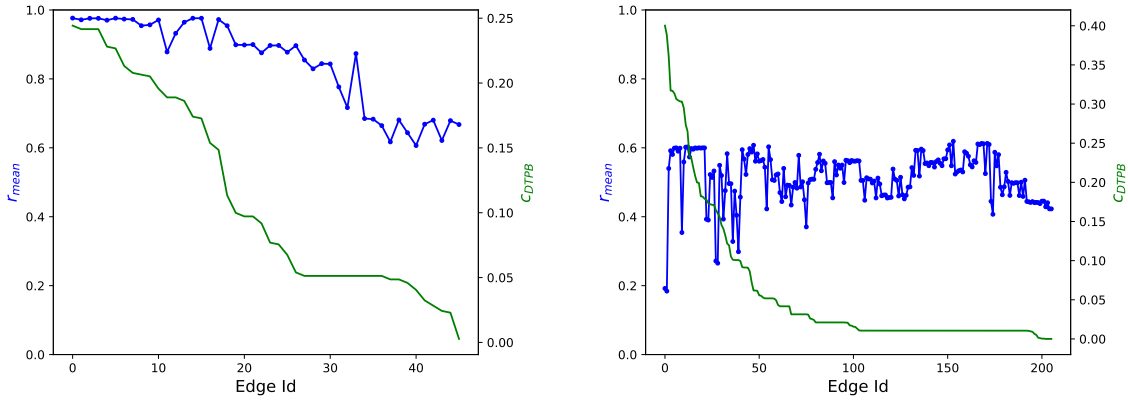

(a) `nesta_case39_epri` (b) `nesta_case189_edin`

Figure 6.6.: The r_{mean}-values compared to c_{DTPB} of a switched edge for two case files. The x-axis shows the switched edges in decreasing order by their c_{DTPB}-values. The left y-axis shows the average mean-field value during the integration (blue line). The y-axis on the right side shows the c_{DTPB}-betweenness values (green line).

The mean-field study was developed for the Kuramoto model but can be used for higher order systems. However, Rodrigues et al. [RPJK16, Sec. 2.1] point out that it was originally defined for fully connected graphs with homogeneous coupling K and could become inaccurate for certain topologies such as heavily clustered networks. Power grids on

the other hand are certainly not all-to-all connected. Nevertheless, Timme used the r_{mean} formulation in [Tim18] to show that the synchronization behavior of the Kuramoto model and the power grid oscillator model behave similarly when using different coupling strengths K. When increasing the strength they show a similar transition from an unsynchronized network towards a synchronized one. In Section 6.3 we have a further look into the dynamical parameters for the model and discuss how they can affect the results.

6.3. Final Remarks

The NESTA dataset our analyses are based on represents a power grid in a static state. In this state the system is in an equilibrium, meaning there is no transient behavior and the phase differences are constant. This steady state is useful for load flow analysis and optimization problems. However, the case files do not provide parameters that only come into play in dynamic analysis, namely the damping α and inertia I that play a role in Equation (4.10). These dynamic parameters can be different for each bus and depend on what properties the connected machines have. The inertia of a large hydro power turbine can be a lot higher that of a gas turbine and so on.
Sadly we were not able to find useful open source data on dynamical properties. Nishikawa et al. [NM15] confirm that these values are not always available but can be computed due to their correlation to the active power output and present an estimation method. However, as this would go beyond the scope of this work we relied on established values from the literature. There are different works available that use differing values. As we saw in Definition 4.1 the inertia term is modeled implicitly by the other system parameters P_i, α and K.
A consistent assumption seems to be to set the damping to $\alpha = 0.1$, see e.g. [FNP08, RSWT13]. When it comes to coupling things are not so obvious anymore and are a matter of study on their own. Often the presented results assume homogeneous coupling as we did, i.e., K_{ij} is the same for all edges $\{i, j\}$ and hence just K is used. A suggestion of Rhoden et al. [RJTK16] is $K = 10\ \mathrm{s}^{-2}$. Schäfer et al. [SWTL18] use values ranging from $K = 5\ \mathrm{s}^{-2}$ to $K = 10\ \mathrm{s}^{-2}$ for different power grids. We eventually settled with a value of $K = 7\ \mathrm{s}^{-2}$ as a compromise but point out that this choice of parameters should be refined further to capture more realistic line parameters. The choice of the power terms P_i again depends on what one wishes to model. Schäfer et al. [SWTL18] start out with setting the power terms uniformly to $P_i = \pm 1.0$ for all generators and loads. This is what we did as well. This can be improved in a next step to model e.g. different kinds sizes of power generators such as a large power plant producing e.g. $P_i = 10.0$ [RSWT13].

Other and more refined system parameters will ultimately lead to a different utilization of the transmission lines and can produce more realistic results. Nevertheless, the produced results can be understood as a first indicator to the effects of DTP-based switchings on dynamical power grids.

Finally, an observation of ours was that phase angle differences and frequency amplitudes sometimes are higher than would be allowed for regular power grid operation (see Table 2.1), but synchronization still took place. This not only happened in our simulations but can be seen as well in the literature, e.g., [WRZ+16a, RSTW12]. The situation in reality may be different since the oscillators' synchronization is self-organized and no primary control is implemented to the net for regulation. Yet, we also have to keep in mind that we only study a simplified model of a very complex system and that the consequences of over- or under frequency wide-ranging effects that the oscillator model cannot capture. This consideration however goes beyond the scope of this theoretical work.

7. Conclusion

In this work we presented a comparative analysis for the switching in static and dynamic power grids based on dominating theta paths. We showed the derivation of the linear DC-model and how it is put to use on graph-theoretic flow networks to find MTSFs. We explained what the limitations of such a static representation are and then introduced the oscillator model with a detailed derivation. We then used small-signal analysis as well as numerical integration on the NESTA dataset in order to get insights into the networks stability and synchronization behavior after switching out an edge. For the evaluation we compared the c_{DTPB} centrality measure [GRW+18] on network edges to several dynamical properties.
Our findings were that the amplitudes of frequency oscillations after removing an edge tend to be smaller in a lot of cases when the edge's c_{DTPB}-value was higher. When looking at small-signal analysis our findings showed that edge switchings with smaller c_{DTPB}-values were more likely to leave the system in a a critical or unstable state. In general our results showed that the removal of the edge with the highest centrality measure almost always leaves the network in an operable state.
Next, we looked at the load redistribution that takes place after an edge has been removed and the power flow had to find new routes from a generator to a load. We observed that edges with a higher centrality in many cases lead to less severe changes in the load of individual edges. Furthermore, we saw that the accumulated load changes over all remaining edges often grew when edges with lower c_{DTPB}-values were removed. This showed the expected inverse proportional behavior. Another finding was that edges whose switchings lead to a critical or unstable state also tend to be affected more by load redistributions. This can be linked to topological properties such as tree edges. A special case is the `nesta_case189_edin` power grid. It contains many tree-like structures with few redundant edges. This had the network more vulnerable to the removal of edges, as it disconnects in a lot of cases with more load redistribution and no synchronization as a consequence. Our results also confirmed this.
Finally, we had a look at the mean-field values of the power grids as another measure for the transient behavior after switching. Again, we could observe that in most cases a lower c_{DTPB}-value can be linked to a reduced phase-coherence.

In conclusion, we were able to compare static and dynamic modeling approaches and could make first connections between the two words. Our findings were that in many cases we can in fact see a correspondence between the c_{DTPB}-value of a switched transmission line in a power grid and measures such as stability, load redistribution and mean-field values. There

are however cases where the absence of redundant edges can cause non-ideal situations and the centrality measure does not correspond to the stability anymore.

7.1. Future Work

It is a tremendous task to take every aspect into account when modeling such a complex system as a power grid. Therefore, we only looked at specific properties using a model based on a range of simplifications. Further work certainly has to contain a refined choice of system parameters for a more realistic representation. Especially the dynamical parameters inertia and damping need to be defined in a way so that they represent the physical machines properly [NM15].
In our approach every node in the network represents either a generator or a load. In real life networks however there are also intermediate buses that neither produce nor consume power that need to be taken care of. The Kron reduction [DB13, GDCB17] is a method applied in network analysis to get rid of such buses while preserving the electrical properties of the original power grid. For more realistic approaches this step should be included in the analysis.
Another extension to small signal analysis is an energy function that can be used to find the stability region of the system [KCG+19]. System states from which convergence towards an equilibrium point is possible lie within this region. It is depending on the initial system configuration as well as the chosen parameters and the structural changes we apply. Knowing it can give further insight on the conditions that have to be met in order for a system to stay stable after switching out edges.

Looking at the topology of the analyzed networks revealed that edges of certain subgraphs such as larger trees are not suited for switchings. Further investigation of substructures such as bridges and clusters promises to give more answers to the question how DTP-betweenness and stable switchings are connected.

Extending the studies to additional datasets may also be of interest. The PyPSA-dataset [BHS18] for example models the high voltage power grids of most European countries. It contains not only static network data but also snapshots of the network operation recorded over an extended period of time. Such data can be used to asses how the switching interventions during regular operation influence the power flow. One can then introduce perturbations in order to simulate load peaks or reduced generation periods in order to study the network resilience to these events after an edge was removed.

Furthermore, an initial idea was to incorporate dynamic behavior to the static graph-theoretic model by using so-called *time-expanded networks*. First introduced by Ford and Fulkerson [FF58] this is an extension to flow networks that considers flows over several time steps instead of only one static instance. It allows to model changing properties of the network such as flow rates, transmission speeds and much more. Although it was successfully applied in many fields [Aro89], so far no application to power grids was made. Discretization of the continuous power flow and handling the fast transmission times of electrical power cause modeling issues. A possible approach to follow would be continuous time-expanded networks [Nas09] where time is continuous and flow problems are solved by giving a discrete approximation of the time-continuous flow.

Bibliography

[Adi00] M.M. Adibi. *Power system restoration: Methodologies & implementation strategies*. 01 2000.

[AM11] K. Ahnert and M. Mulansky. Odeint - solving ordinary differential equations in c++. In *AIP Conf. Proc. 1389*, pages 1586–1589, 2011.

[APV79] T. Athay, R. Podmore, and S. Virmani. A practical method for the direct analysis of transient stability. *IEEE Transactions on Power Apparatus and Systems*, PAS-98(2):573–584, 1979.

[AR15] Ali R. Al-Roomi. Power flow test systems repository. `https://al-roomi.org/multimedia/Power_Flow/14BusSystem/IEEE14BusSystem.tiff`, 2015.

[Aro89] Jay E. Aronson. A survey of dynamic network flows. *Annals of Operations Research*, 20(1):1–66, dec 1989.

[BHS18] T. Brown, J. Hörsch, and D. Schlachtberger. PyPSA: Python for Power System Analysis. *Journal of Open Research Software*, 6(4), 2018.

[Blu06] Seth Blumsack. *Network topologies and transmission investment under electric-industry restructuring*. PhD thesis, 2006.

[BPG01] S. Binato, M. V. F. Pereira, and S. Granville. A new benders decomposition approach to solve power transmission network design problems. *IEEE Transactions on Power Systems*, 16(2):235–240, 2001.

[Bra68] D. Braess. Über ein Paradoxon aus der Verkehrsplanung. *Unternehmensforschung Operations Research - Recherche Opérationnelle*, 12(1):258–268, dec 1968.

[CGS14] Carleton Coffrin, Dan Gordon, and Paul Scott. NESTA, The NICTA Energy System Test Case Archive. nov 2014.

[DB13] Florian Dörfler and Francesco Bullo. Kron reduction of graphs with applications to electrical networks. *IEEE Transactions on Circuits and Systems I: Regular Papers*, 60(1):150–163, feb 2013.

[Die05] Reinhard Diestel. *Graph Theory (Graduate Texts in Mathematics)*. Springer, August 2005.

[faz06] „dominoeffekt“ nach menschlichem versagen. *Frankfurter Allgemeine Zeitung*, Nov 2006.

[FF58] L. R. Ford and D. R. Fulkerson. Constructing Maximal Dynamic Flows from Static Flows. *Operations Research*, 6(3):419–433, 1958.

[FNP08] G. Filatrella, A. H. Nielsen, and N. F. Pedersen. Analysis of a power grid using a Kuramoto-like model. *The European Physical Journal B*, 61(4):485–491, feb 2008.

[FOF08] Emily B. Fisher, Richard P. O'Neill, and Michael C. Ferris. Optimal transmission switching. *IEEE Transactions on Power Systems*, 23(3):1346–1355, 2008.

[G+18] M. Galassi et al. Gnu scientific library reference manual. `https://www.gnu.org/software/gsl/`, 2018.

[GDCB17] Colin Grudzien, Deepjyoti Deka, Michael Chertkov, and Scott N Backhaus. Structure- & Physics- Preserving Reductions of Power Grid Models. jul 2017.

[GJ+10] Gaël Guennebaud, Benoît Jacob, et al. Eigen v3. `http://eigen.tuxfamily.org`, 2010.

[GMM92] F. D. Galiana, D. T. McGillis, and M. A. Marin. Expert systems in transmission planning. *Proceedings of the IEEE*, 80(5):712–726, 1992.

[GRW+18] Alban Grastien, Ignaz Rutter, Dorothea Wagner, Franziska Wegner, and Matthias Wolf. The Maximum Transmission Switching Flow Problem. pages 340–360, 2018.

[GSO12] Duncan Glover, Mulukutla Sarma, and Thomas Overbye. *Power System Analysis & Design*, volume 53. 2012.

[H+07] B. Holger et al. Transmissioncode 2007. `https://www.n-ergie-netz.de/public/remotemedien/media/mdn/produkte_und_dienstleistungen/netzanschluss/gesetze/070801TransmissionCode_20072.pdf`, 2007.

[HvBG+10] Dominik Heide, Lueder von Bremen, Martin Greiner, Clemens Hoffmann, Markus Speckmann, and Stefan Bofinger. Seasonal optimal mix of wind and solar power in a future, highly renewable Europe. *Renewable Energy*, 35(11):2483–2489, nov 2010.

[KBL94] P. Kundur, N.J. Balu, and M.G. Lauby. *Power System Stability and Control*. EPRI power system engineering series. McGraw-Hill Education, 1994.

[KCG+19] Michael Kyesswa, Huseyin K. Cakmak, Lutz Groll, Uwe Kuhnapfel, and Veit Hagenmeyer. A hybrid analysis approach for transient stability assessment in power systems. In *2019 IEEE Milan PowerTech, PowerTech 2019*. Institute of Electrical and Electronics Engineers Inc., jun 2019.

[KPA+04] P. Kundur, J. Paserba, V. Ajjarapu, G. Andersson, A. Bose, C. Canizares, N. Hatziargyriou, D. Hill, A. Stankovic, C. Taylor, T. Van Cutsem, and V. Vittal. Definition and Classification of Power System Stability IEEE/CIGRE Joint Task Force on Stability Terms and Definitions. *IEEE Transactions on Power Systems*, 19(3):1387–1401, aug 2004.

[Kru18] Florian Krueger. A block-cut-tree-based switching algorithm for cacti, 2018.

[Kur75] Yoshiki Kuramoto. Self-entrainment of a population of coupled non-linear oscillators. In *International Symposium on Mathematical Problems in Theoretical Physics*, volume 39, pages 420–422. Springer-Verlag, Berlin/Heidelberg, 1975.

[Kur03] Yoshiki Kuramoto. *Chemical oscillations, waves, and turbulence*. Courier Corporation, 2003.

[LBDG12] S. Lozano, L. Buzna, and A. Díaz-Guilera. Role of network topology in the synchronization of power systems. *European Physical Journal B*, 85(7), 2012.

[LGHV15] Karsten Lehmann, Alban Grastien, Pascal Van Hentenryck, and Pascal Van Hentenryck. The Complexity of Switching and FACTS Maximum-Potential-Flow Problems. *CoRR*, abs/1507.0, 2015.

[LGV14] Karsten Lehmann, Alban Grastien, and Pascal Van Hentenryck. The Complexity of DC-Switching Problems. *CoRR*, abs/1411.4:1–14, 2014.

[LGV16] Karsten Lehmann, Alban Grastien, and Pascal Van Hentenryck. AC-Feasibility on Tree Networks is NP-Hard. *IEEE Transactions on Power Systems*, 31(1):798–801, 2016.

[LK07] G. A. LEONOV and N. V. KUZNETSOV. Time-varying linearization and the perron effects. *International Journal of Bifurcation and Chaos*, 17(04):1079–1107, 2007.

[LMM+15] Thomas Leibfried, Tamara Mchedlidze, Nico Meyer-Hübner, Martin Nöllenburg, Ignaz Rutter, Peter Sanders, Dorothea Wagner, and Franziska Wegner. Operating power grids with few flow control buses. *CoRR*, abs/1505.05747, 2015.

[mdr19] Suedlink: Ein 320.000-volt-erdkabel mitten durch deutschland. *MDR*, Apr 2019.

[ML02] Adilson E. Motter and Ying Cheng Lai. Cascade-based attacks on complex networks. *Physical Review E - Statistical Physics, Plasmas, Fluids, and Related Interdisciplinary Topics*, 66(6):4, dec 2002.

[MV06] Oliver Mason and Mark Verwoerd. Graph Theory and Networks in Biology. *IET Systems Biology*, 1(2):89–119, mar 2006.

[Nas09] Ebrahim Nasrabadi. *Dynamic Flows in Time-varying Networks*. PhD thesis, 2009.

[NM15] Takashi Nishikawa and Adilson E. Motter. Comparative analysis of existing models for power-grid synchronization. *New Journal of Physics*, 17, jan 2015.

[PAH14] T. Pesch, H.-J. Allelein, and J.-F. Hake. Impacts of the transformation of the German energy system on the transmission grid. *The European Physical Journal Special Topics*, 223(12):2561–2575, oct 2014.

[pi-] P-section equivalent circuits. "`https://www.pscad.com/webhelp/EMTDC/Transmission_Lines/PI-Section_Equivalent_Circuits.htm`".

[PMVB05] K. Purchala, L. Meeus, D. Van Dommelen, and R. Belmans. Usefulness of DC power flow for active power flow analysis. *IEEE Power Engineering Society General Meeting, 2005*, pages 2457–2462, 2005.

[PTVF07] William H. Press, Saul A. Teukolsky, William T. Vetterling, and Brian P. Flannery. *Numerical Recipes 3rd Edition: The Art of Scientific Computing*. Cambridge University Press, 3 edition, 2007.

[RJTK16] Martin Rohden, Daniel Jung, Samyak Tamrakar, and Stefan Kettemann. Cascading failures in AC electricity grids. *Physical Review E*, 94(3):1–8, 2016.

[RPJK16] Francisco A. Rodrigues, Thomas K.D.M. Peron, Peng Ji, and Jürgen Kurths. The Kuramoto model in complex networks, jan 2016.

[RSTW12] Martin Rohden, Andreas Sorge, Marc Timme, and Dirk Witthaut. Self-organized synchronization in decentralized power grids. *Physical Review Letters*, 109(6):1–5, 2012.

[RSWT13] Martin Rohden, Andreas Sorge, Dirk Witthaut, and Marc Timme. Impact of network topology on synchrony of oscillatory power grids. may 2013.

[SAMS04] Ingve Simonsen, Kasper Astrup Eriksen, Sergei Maslov, and Kim Sneppen. Diffusion on complex networks: a way to probe their large-scale topological structures. *Physica A: Statistical Mechanics and its Applications*, 336(1-2):163–173, may 2004.

[SBP+08] Ingve Simonsen, Lubos Buzna, Karsten Peters, Stefan Bornholdt, and Dirk Helbing. Transient dynamics increasing network vulnerability to cascading failures. *Physical Review Letters*, 100(21):1–4, 2008.

[Sch14] Boris Schäling. *The boost C++ libraries*. XML Press, 2014.

[Sim05] Ingve Simonsen. Diffusion and networks: A powerful combination! *Physica A: Statistical Mechanics and its Applications*, 357(2):317–330, nov 2005.

[SR70] Fred C. Schweppe and Douglas B. Rom. Power System Static-State Estimation, Part II: Approximate Model. *IEEE Transactions on Power Apparatus and Systems*, PAS-89(1):125–130, jan 1970.

[SRM+18] Konstantin Sharafutdinov, Leonardo Rydin Gorjão, Moritz Matthiae, Timm Faulwasser, and Dirk Witthaut. Rotor-angle versus voltage instability in the third-order model for synchronous generators. *Chaos*, 28(3), 2018.

[Sto74] Brian Stott. Review of Load-Flow Calculation Methods. *Proceedings of the IEEE*, 62(7):916–929, 1974.

[Str00] Steven H. Strogatz. From Kuramoto to Crawford: Exploring the onset of synchronization in populations of coupled oscillators. *Physica D: Nonlinear Phenomena*, 143(1-4):1–20, sep 2000.

[SWTL18] Benjamin Schäfer, Dirk Witthaut, Marc Timme, and Vito Latora. Dynamically induced cascading failures in power grids. *Nature Communications*, 9(1), 2018.

[Tim18] Marc Timme. *Collective Dynamics of Power Grids –Paradoxes and Challenges for Data Analysis and Modeling*, pages 231–260. BIS-Verlag der Carl von Ossietzky Universität Oldenburg, Oldenburg, 2018.

[UoW14] Department of Electrical Engineering University of Washington. Power systems test case archive, 2014. `http://www.ee.washington.edu/research/pstca/`, accessed 2014-12-2.

[Weg19] Franziska Wegner. Combinatorial problems in energy networks — graph-theoretic models and algorithms, 2019. To appear.

[Win19] Lena Winter. Transmission network expansionplanning for curing critical edges, 2019.

[WJSO12] Tilman Weckesser, Hjortur Johannsson, Stefan Sommer, and Jacob Ostergaard. Investigation of the adaptability of transient stability assessment methods to real-time operation. *IEEE PES Innovative Smart Grid Technologies Conference Europe*, 2012.

[WRZ+16a] Dirk Witthaut, Martin Rohden, Xiaozhu Zhang, Sarah Hallerberg, and Marc Timme. Critical Links and Nonlocal Rerouting in Complex Supply Networks. *Physical Review Letters*, 116(13), mar 2016.

[WRZ+16b] Dirk Witthaut, Martin Rohden, Xiaozhu Zhang, Sarah Hallerberg, and Marc Timme. Critical Links and Nonlocal Rerouting in Complex Supply Networks - Supporting Information. Technical report, 2016.

[WT12] Dirk Witthaut and Marc Timme. Braess's paradox in oscillator networks, desynchronization and power outage. *New Journal of Physics*, 14, 2012.

[ZMsT+11] Ray Daniel Zimmerman, Carlos Edmundo Murillo-sánchez, Robert John Thomas, Ray Daniel Zimmerman, Carlos Edmundo Murillo-sánchez, Robert John Thomas, and Life Fellow. MATPOWER: Steady-state operations, planning, and analysis tools for power systems research and education. *IEEE TRANSACTIONS ON POWER SYSTEMS*, 26(1):12—-19, feb 2011.

Appendix

A. Additional Results

In this chapter we present some additional plots to accompany the results and discussion of Chapter 6. Figure A.1 shows our findings for the comparison of the c_{DTPB}-values with the stability results of the small-signal analysis. Figure A.2 shows results for additional case files on the accumulated load differences. Figure A.3 shows additional results for the comparison of mean-field values and the c_{DTPB}-values.

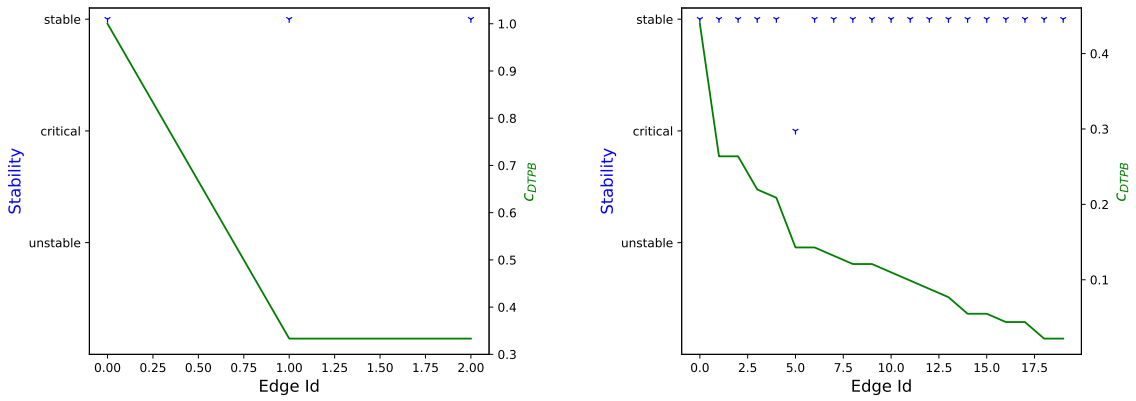

(a) `nesta_case3_lmbd`

(b) `nesta_case14_ieee`

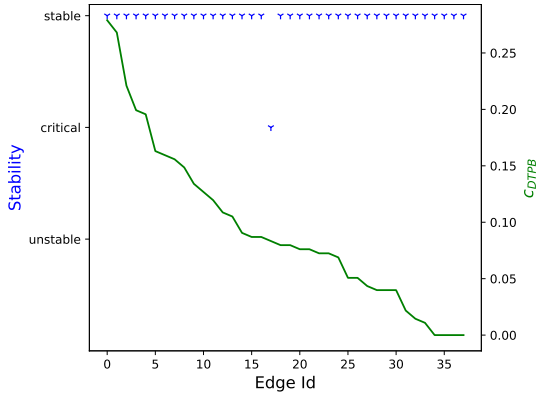

(c) `nesta_case24_ieee_rts`

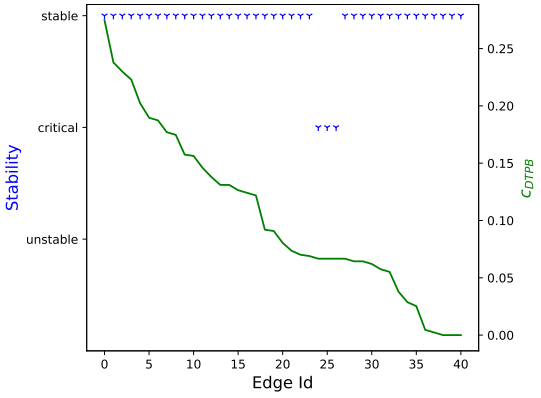

(d) `nesta_case30_ieee`

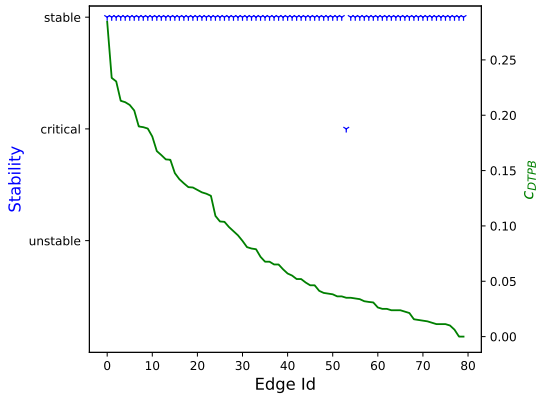

(e) `nesta_case57_ieee`

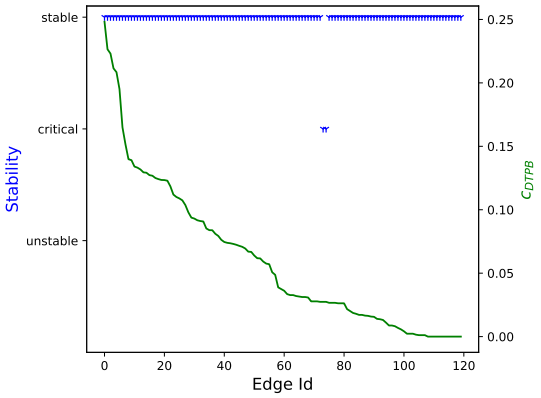

(f) `nesta_case73_ieee_rts`

Figure A.1.: Stability compared to the DTP-betweenness of an edge. The x-axis shows which edge is switched out where the edges are ranked in decreasing order by their c_{DTPB}-values. The left y-axis shows the three possible stability states of the small-signal analysis (blue dots). The y-axis on the right side shows the c_{DTPB}-values (green line).

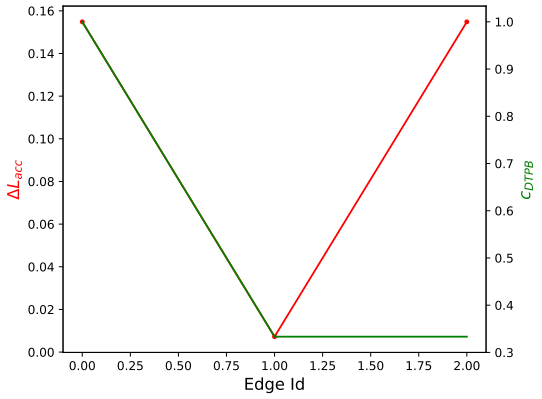

(a) `nesta_case3_lmbd`

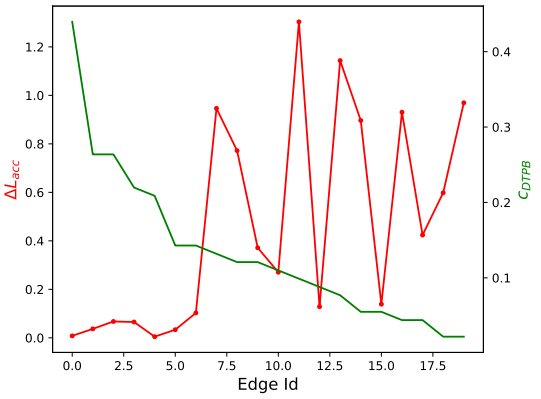

(b) `nesta_case14_ieee`

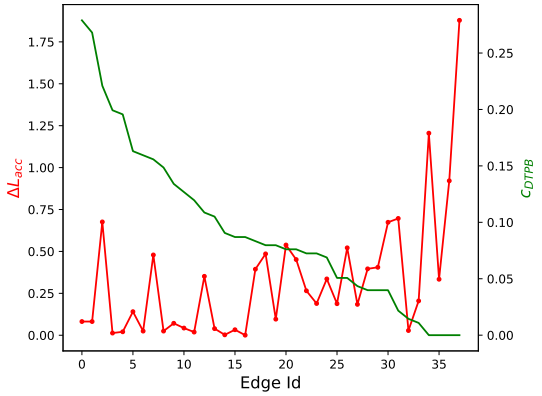

(c) `nesta_case24_ieee_rts`

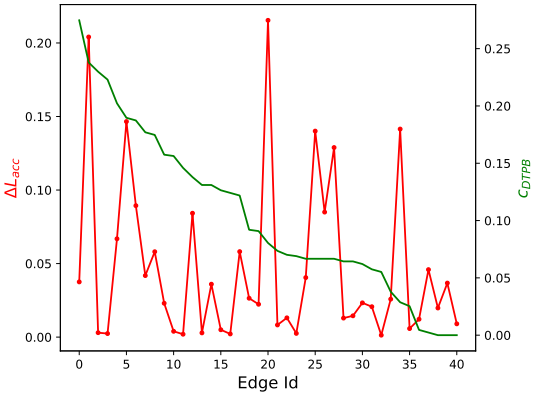

(d) `nesta_case30_ieee`

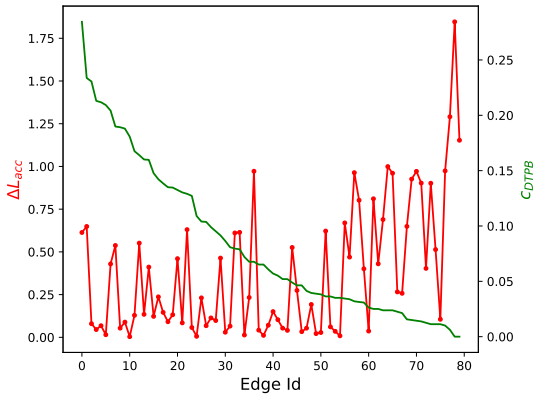

(e) `nesta_case57_ieee`

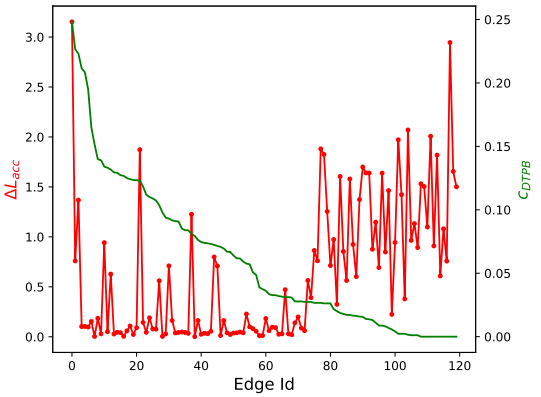

(f) `nesta_case73_ieee_rts`

Figure A.2.: Load difference in comparison to c_{DTPB}-values. The x-axis shows the switched edges in decreasing order by their c_{DTPB}-values. The left y-axis shows represents the $\Delta L_{ij_{acc}}$-values (red line). The y-axis on the right side shows the c_{DTPB}-values (green line).

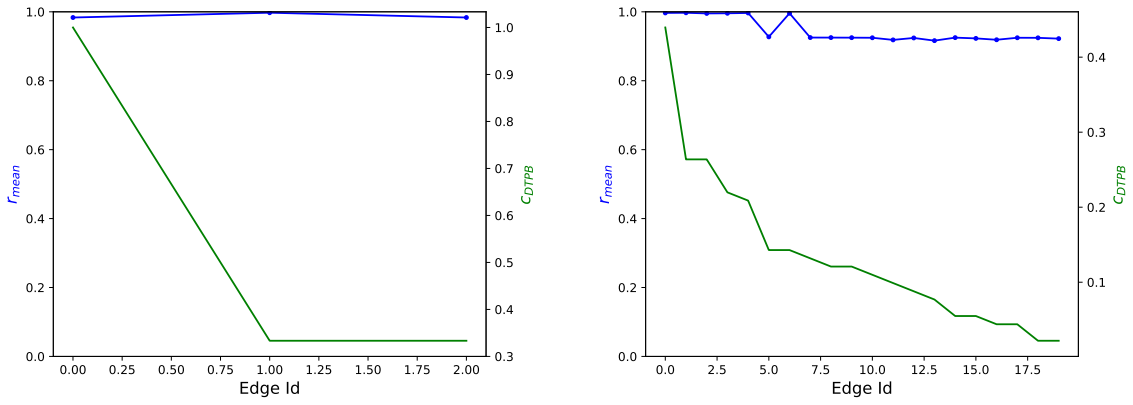

(a) `nesta_case3_lmbd`

(b) `nesta_case14_ieee`

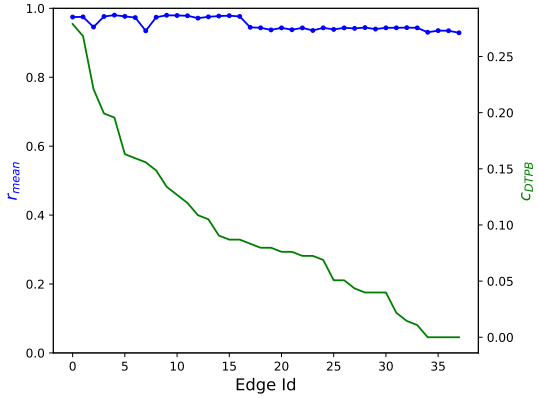

(c) `nesta_case24_ieee_rts`

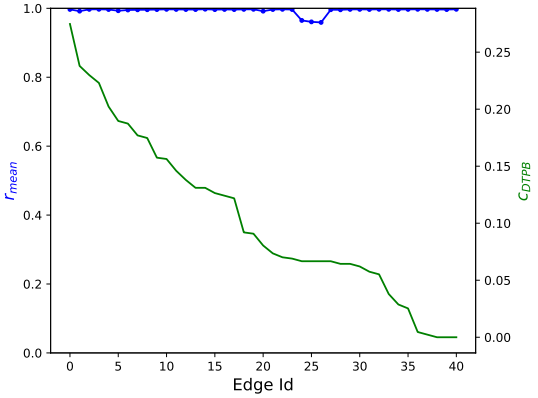

(d) `nesta_case30_ieee`

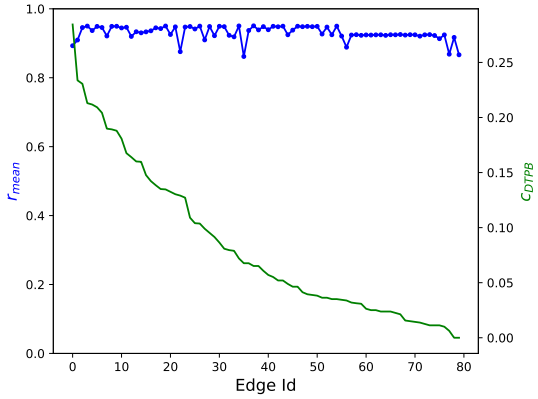

(e) `nesta_case57_ieee`

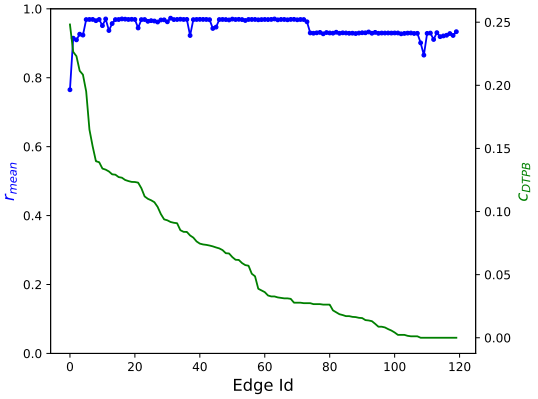

(f) `nesta_case73_ieee_rts`

Figure A.3.: The r_{mean}-value compared to c_{DTPB} of a switched edge. The x-axis shows the switched edges in decreasing order by their c_{DTPB}-values. The left y-axis shows the average mean-field value during the integration (blue line). The y-axis on the right side shows the c_{DTPB}-betweenness values (green line).